CHALMERS
UNIVERSITY OF TECHNOLOGY

Development of a Computationally Efficient Tabulated Chemistry Solver for Internal Combustion Engine Optimization Using Stochastic Reactor Models

Downloaded from: https://research.chalmers.se, 2021-08-31 11:39 UTC

Citation for the original published paper (version of record):

Matrisciano, A., Franken, T., Gonzalez Mestre, L. et al (2020)
Development of a Computationally Efficient Tabulated Chemistry Solver for Internal Combustion Engine Optimization Using Stochastic Reactor Models
Applied Sciences, 10(24): 1-31
http://dx.doi.org/10.3390/app10248979

N.B. When citing this work, cite the original published paper.

research.chalmers.se offers the possibility of retrieving research publications produced at Chalmers University of Technology.
It covers all kind of research output: articles, dissertations, conference papers, reports etc. since 2004.
research.chalmers.se is administrated and maintained by Chalmers Library

(article starts on next page)

applied sciences

MDPI

Article

Development of a Computationally Efficient Tabulated Chemistry Solver for Internal Combustion Engine Optimization Using Stochastic Reactor Models

Andrea Matrisciano [1,2,*], Tim Franken [3], Laura Catalina Gonzales Mestre [3], Anders Borg [1] and Fabian Mauss [3]

1 Lund Combustion Engineering LOGE AB, Scheelevägen 17, 22370 Lund, Sweden; anders.borg@logesoft.com
2 Department of Mechanics and Maritime Sciences, Division of Combustion and Propulsion Systems, Chalmers University of Technology, Horsalvägen 7a, 41296 Gothenburg, Sweden
3 Thermodynamics and Thermal Process Engineering, Brandenburg University of Technology Cottbus, Senftenberg, Siemens-Halske-Ring 8, 03046 Cottbus, Germany; Tim.Franken@b-tu.de (T.F.); LauraCatalina.GonzalezMestre@b-tu.de (L.C.G.M.); FMauss@b-tu.de (F.M.)
* Correspondence: andmatr@chalmers.se; Tel.: +46-7-0863-0560

Received: 28 October 2020; Accepted: 8 December 2020; Published: 16 December 2020

Abstract: The use of chemical kinetic mechanisms in computer aided engineering tools for internal combustion engine simulations is of high importance for studying and predicting pollutant formation of conventional and alternative fuels. However, usage of complex reaction schemes is accompanied by high computational cost in 0-D, 1-D and 3-D computational fluid dynamics frameworks. The present work aims to address this challenge and allow broader deployment of detailed chemistry-based simulations, such as in multi-objective engine optimization campaigns. A fast-running tabulated chemistry solver coupled to a 0-D probability density function-based approach for the modelling of compression and spark ignition engine combustion is proposed. A stochastic reactor engine model has been extended with a progress variable-based framework, allowing the use of pre-calculated auto-ignition tables instead of solving the chemical reactions on-the-fly. As a first validation step, the tabulated chemistry-based solver is assessed against the online chemistry solver under constant pressure reactor conditions. Secondly, performance and accuracy targets of the progress variable-based solver are verified using stochastic reactor models under compression and spark ignition engine conditions. Detailed multicomponent mechanisms comprising up to 475 species are employed in both the tabulated and online chemistry simulation campaigns. The proposed progress variable-based solver proved to be in good agreement with the detailed online chemistry one in terms of combustion performance as well as engine-out emission predictions (CO, CO_2, NO and unburned hydrocarbons). Concerning computational performances, the newly proposed solver delivers remarkable speed-ups (up to four orders of magnitude) when compared to the online chemistry simulations. In turn, the new solver allows the stochastic reactor model to be computationally competitive with much lower order modeling approaches (i.e., Vibe-based models). It also makes the stochastic reactor model a feasible computer aided engineering framework of choice for multi-objective engine optimization campaigns.

Keywords: tabulated chemistry; chemical kinetics; 0-D stochastic reactor models

1. Introduction

The ever-stringent regulations on carbon dioxide and criteria pollutants (i.e., nitrogen oxides or particulate matter) for internal combustion engine vehicles (ICEV), as well as the original equipment manufacturers (OEM) needing to reduce the technology development times, are among the key drivers of modern computer aided engineering (CAE) for engine development toolchains. To thoroughly

study and optimize engine fuel efficiency and reduce pollutant formation, an experimentally driven campaign generally requires the deployment of expensive and highly complex techniques. Moreover, the ever-increasing hardware complexities being introduced in modern powertrains (i.e., pre-chamber or advanced multi-stage aftertreatment) make the experimental engine development process even more challenging. Each new technology introduces a new degree of freedom in the parameter range of a combustion engine development. In this scenario, numerical methods represent an attractive tool to aid the engine development process, more so if they are capable of accounting for both the chemical and physical phenomena occurring in an internal combustion engine-based powertrain. Provided that such numerical methods deliver an acceptable level of accuracy, engine development costs can be substantially reduced by running engine optimization campaigns within a virtual framework. However, modeling of the in-cylinder combustion process poses many challenges, such as (1) Turbulence-Chemistry Interaction (TCI), (2) fuel injection and mixture formation and (3) gaseous pollutants and particulates formation mechanisms. On top of the numerical complexity, computational cost is also among the major decisive factors of whether a certain modeling approach shall be deployed in the development stage or not. The methods need to be fast to deliver information in time during an engine or vehicle development process.

Among the different reactive flow simulation frameworks currently adopted for engine development, 3-D Computational Fluid Dynamics (CFD) allows to model flow, turbulence and combustion chemistry processes with high level of detail. However, depending on the chosen model parameters such as computational grid/time-step size, numerical differencing scheme and the number of species/reactions in the chosen chemical kinetic model, 3-D CFD may require an unfeasible computational cost. This is particularly true when engine and fuel chemistry effects are to be considered across a large set of operating points or during transient operations. In this respect, lower order tool chains (i.e., 0-D and 1-D frameworks) require a small fraction of the computational times compared to advanced 3-D CFD analyses. The price for this benefit is the limited numerical accuracy and frequently a loss of chemical and physical information. The treatment of the combustion chemistry and the turbulence-chemistry interaction effects are among the main aspects to be addressed in order to achieve high accuracy and feasible simulation times. Both these phenomena become particularly important in the development and optimization of novel internal combustion engine concepts which may include, for instance, dual-fuel, highly premixed fuel/oxidizer mixtures or complex exhaust gas recirculation (EGR) strategies.

Numerous 0-D methods have been proposed to describe the Rate of Heat Release (RoHR) and the turbulence for both Spark Ignition (SI) and Compression Ignition (CI) engines to with different level of complexity [1–6].

In addition to the turbulence/burn rate interaction, the computational treatment of in-homogeneities in the combustion chamber can strongly affect the predictive capability of a 0-D model especially under Diesel engine conditions. The most common approach is to discretize the trapped mass into several computational zones, which vary depending on the number of physical regions included in the model formulation (i.e., flame front, cylinder wall area, crevice [7–11]). While such models present a remarkable advantage against single or two zone models, a mean temperature and gas composition within each zone has still to be imposed by definition. This implies that the calculation of the chemical source terms is done assuming negligible variations in enthalpy and composition spaces within each zone and hence no TCI effects are considered. These simplifications, together with the lack of detailed chemistry sub-models, impact the quality of engine-out emission predictions.

An alternative method to consider turbulent mixing as well as detailed chemistry in 0-D is the Stochastic Reactor Model (SRM). The SRM discretizes the mixture in the combustion chamber in a given number of notional particles under the assumption of statistical homogeneity, as opposed to special homogeneity in multi-zone models. Each notional particle features a realization of possible temperature and mixture compositions. TCI is mimicked by stochastic mixing of particles, stochastic heat exchange with the walls and detailed chemistry evaluations. However, as it is the case for detailed

chemistry-based 3-D CFD methods, depending on the size of the chemical mechanism considered, the chemistry step may take up to 99% of the simulation time. In addition to mechanism reduction techniques [12], chemistry storage and run-time retrieval methods are viable solutions to reduce computational costs.

Different tabulated chemistry-based methods have been proposed primarily for 3-D CFD applications. These methodologies are based on the decoupling of flow and chemistry. While the flow is computed during run-time, the chemistry solution, usually intended as auto-ignition and/or emission formation processes, is computed in a pre-processing step typically performed on a one-time basis for a given fuel. The two major combustion modeling concepts used to decouple flow and chemistry are various flamelet methods, including Conditional Moment Closure (CMC) and the Well-Stirred Reactor (WSR) methods. Remarkable efforts have been made towards formulation of predictive flamelet-based tabulated chemistry solvers for auto-ignition [13–17] as well as advanced soot and NO_x emission formation modeling [18–21]. The present article is based on the WSR approach. This is the best choice for Probability Density Function (PDF) methods, such as the herein employed SRM. These methods use operator splitting loops to separate vaporization, mixing, compression, heat transfer and chemistry. In these processes, each particle is considered as a well stirred reactor. The chemistry storage is constructed by means of 0-D adiabatic constant pressure/volume reactors across wide ranges of initial pressure, temperature and equivalence ratio. Pires da Cruz et al. [22] proposed a method where both the high and low temperature ignition delay times are stored in the look-up table. The validation was done under 0-D adiabatic reactor conditions (assuming constant pressure/volume) as well as under diesel engine conditions in 3-D CFD. An improved version of such model was later proposed by Colin et al. [23] where a progress-variable-based approach was used rather than a tabulation of the ignition delays. In this configuration, an additional tabulation dimension is introduced as the tabulation is done across a predefined set of grid points, varying between unburned and fully burned mixture. During run-time, the progress variable source term was retrieved for each cell, and it was used to reconstruct the chemical state. Later improvements of such method proposed by Knop and co-authors [24] also incorporated a turbulence-chemistry interaction term during the tabulation process. Thanks to an additional tabulation dimension, TCI effects could be accounted for in 3-D CFD reactive flow simulations within the Extended Coherent Flame Model (ECFM) framework. The model (referred as ECFM-TKI in [24]) has been applied to predict the ignition process of Diesel and homogeneous charge compression ignition (HCCI) engines and is currently implemented in various commercial engine CFD software.

With respect to modeling of spray flames and Diesel engines, numerous models, such as the Partially Stirred Reactor (PaSR) concept [25], have been formulated and implemented in OpenFOAM [26,27].

When it comes 0-D/1-D frameworks, the number of studies featuring tabulated chemistry-based methods is rather limited. Its implementation, however, is potentially very useful as it allows to include detailed chemistry effects, as opposed to the commonly used empirically derived correlations for emission predictions. Leicher et al. [28] proposed a table look-up approach based on mixture fraction and reaction entropy as progress variable. Their methodology was implemented in an SRM and tested under constant pressure reactor conditions. Bernard and co-authors [10] simulated heat release and pollutant formation by means of a Flame Prolongation of Intrinsic Low Dimensional Manifold (FPI/ILDM initially proposed in [29]) as well as a timescale-based sub-model for NO formation. The tabulation method used constant volume reactors and a CO-CO_2-based progress variable definition. Upon table generation, CO, CO_2, H, H_2 and the fuel molecule were stored as key species for the reconstruction of the thermodynamic state during engine simulation. The method was validated for a wide range of Diesel engine conditions. Within the SI engine simulation framework, Bougrine et al. [30] proposed a two-zone 0-D model (referenced as One-Dimensional Coherent Flame Model-Tabulated Chemistry (CFM1D-TC)) where the chemical part of the combustion process was tabulated using laminar 1-D premixed flame solutions. In addition, a time-scale model was formulated to better represent the relaxation towards equilibrium of CO and NO species with the help of homogeneous

reactor calculations. Bozza et al. [31] implemented the previously mentioned ECFM-TKI [24] approach within a 0-D/1-D phenomenological combustion model for better knock prediction in spark ignited engines compared to the traditionally used Livengood-Wu [32] approach. Validation under both 0-D reactors and knocking SI engine simulations under stoichiometric conditions showed promising results when compared to the online chemistry solutions.

Motivation

The present work aims to (1) introduce and validate an improved version of the tabulated chemistry solver initially presented in [33]; (2) assess the solvers' combustion and emissions predictions under Diesel and gasoline engine conditions within the 0-D SRM framework; (3) demonstrate the computational efficiency of the method, which allows large design optimization studies while taking detailed chemistry effects into account. With respect to the analyses discussed in [33], the present work includes numerous performance and accuracy refinements on both the tabulation and the engine simulation codes, phenomenological formulations of the turbulence models for CI and SI engines, a novel approach for thermal NO source terms tabulation and a method validation under SI engine conditions in addition to a broader CI engine simulation campaign. To the authors' knowledge, a comprehensive SRM-based tool chain featuring tabulated chemistry, physical turbulence models and computational efficiency comparable to multi-zone models (i.e., [7]) has not been demonstrated before.

The paper is structured as follows: In Section 2, a concise description of the SRM framework is given together with a description of the turbulence models and progress variable-based solver. In Section 3, an accuracy assessment investigation of the refined storage/retrieval strategy under zero-dimensional constant pressure reactors in shown. The validation of the development is demonstrated in Sections 4–6. Online and tabulated chemistry-based solvers are compared using the SRM under Diesel (Section 4) and spark ignited engine (Section 5) conditions. Finally, the accuracy of the introduced solvers is discussed with focus on combustion and emissions predictions along with remarks on computational performances in Section 6. For validation, the following criteria were defined: (1) Is the solver accuracy consistent with the general model accuracy? (2) Is the CPU time of the developed software acceptable for engine development, engine optimization and driving cycle analysis?

2. Simulation Methods

The SRM has been coupled with two different chemistry solvers: (1) online, where chemical source terms are calculated during run-time; (2) Combustion Progress Variable (CPV), which uses a pre-calculated look-up table to retrieve the source terms for combustion as well as thermal NO formation. In the first sub-section, a brief description of the SRM engine modelling framework is presented for better readability. In the following sub-sections, aspects of the different phenomenological turbulence models adopted for the SI and CI simulation campaigns are briefly presented as well as a description of the tabulated chemistry solver.

2.1. The Stochastic Reactor Model

In the SRM computational domain, the in-cylinder trapped mass is discretized as an ensemble of notional particles that can mix with each other and exchange heat with the cylinder walls. A schematic visualization of the concept, along with an exemplary distribution of the particles' property (i.e., enthalpy or gas composition) is shown in Figure 1. Depending on the initial conditions assigned at Intake Valve Closure (IVC), a given chemical composition, temperature, and mass are assigned to each particle, while pressure is assumed to be the same across all particles.

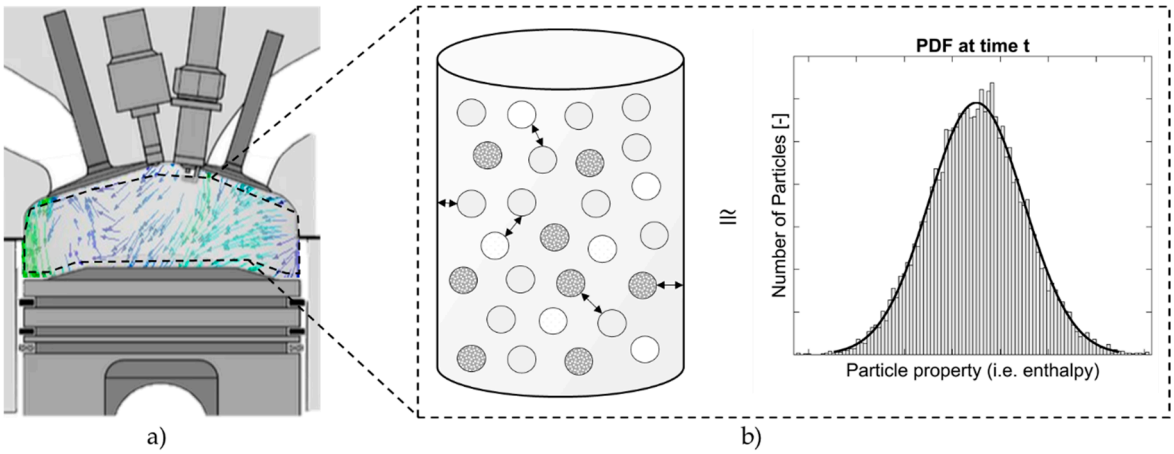

Figure 1. Schematic visualization of the Stochastic Reactor Model (SRM) concept; (**a**) engine physical space; (**b**) 0-D particles in the SRM computational space and an exemplary distribution of particle properties at a given time-step t.

A probability density function is used to describe the in-cylinder content and each particle contributes to the realization of the given PDF at each time-step. Since all stochastic particles in the SRM represent a portion of the in-cylinder mass, a Mass Density Function (MDF) is used to solve the main transport equation of the 0-D SRM. The joint scalar vector of the MDF can be expressed as reported in Equation (1).

$$F_{\mathbf{\Phi}}(\boldsymbol{\psi}, t) = F_{\mathbf{\Phi}}\left(\psi_1, \ldots, \psi_{N_{Sc}}; t\right) \tag{1}$$

The vector $\boldsymbol{\psi}$ is the realization of the vector of local scalar variables noted herein as $\mathbf{\Phi}$, while N_{Sc} is the number of scalars transported in the computational domain. Depending on the chemistry solver used in the simulation framework, the number and type of transported scalars varies significantly.

$$\text{Online chemistry solver } \mathbf{\Phi}(t) = \left(Y_1, Y_2, \ldots, Y_{N_{Sp}}, h; t\right) \tag{2}$$

$$\text{Tabulated chemistry solver (CPV) } \mathbf{\Phi}(t) = \left(\phi, h, w_q, \mathbf{T_p}, yEGR, h_{298}; t\right) \tag{3}$$

In the online chemistry solver formulation (see Equation (2)), the specific enthalpy (h) as well as the full vector of species mass fractions **Y** must be transported in order to correctly compute the chemical reactions during run time. The size of the mass fraction vector is therefore dependent on the number of species (N_{Sp}) defined in the chemical mechanism adopted. With respect to the tabulated chemistry solver, only a reduced set of quantities need to be transported in the computational domain independently on the size of the mechanism used to generate the look-up table. These are the equivalence ratio (ϕ), the specific enthalpy (h), the mean molecular weight (w_q), the vector ($\mathbf{T_p}$) containing the thermodynamic polynomial coefficients, the EGR mass fraction (yEGR) and the latent enthalpy (h_{298}) of the in-cylinder mixture. Once initial conditions are assigned, the transport equation of the joint scalar vector of the MDF is numerically solved using a Monte Carlo particle method (e.g., Pope [34]) with the operator splitting technique as previously presented by Maigaard et al. [35]. A series of sub-models are employed to sequentially solve the different physical and chemical processes occurring in the combustion chamber, as summarized in Equation (4):

$$\frac{\partial F_{\mathbf{\Phi}}}{\partial t} = \left.\frac{\partial F_{\mathbf{\Phi}}}{\partial t}\right|_{\Delta V} + \left.\frac{\partial F_{\mathbf{\Phi}}}{\partial t}\right|_{inj} + \left.\frac{\partial F_{\mathbf{\Phi}}}{\partial t}\right|_{FP} + \left.\frac{\partial F_{\mathbf{\Phi}}}{\partial t}\right|_{mix} \left.\frac{\partial F_{\mathbf{\Phi}}}{\partial t}\right|_{chem} + \left.\frac{\partial F_{\mathbf{\Phi}}}{\partial t}\right|_{ht} \tag{4}$$

In the equation above, the subscript ΔV represents the piston movement, inj fuel injection, FP flame propagation (considered only for SI engine simulations), mix the turbulence and particle interaction process, chem the chemical reactions and ht heat transfer to the walls. Detailed descriptions of the

sub-models used for piston movement, pressure correction, online chemistry solver and fuel injection can be found in the work from Tuner [36]. The treatment of the flame propagation has been previously introduced by Bjerkborn et al. [37] and broadly validated by Pasternak et al. [38] and Netzer [39]. The Woschni model [40] is used to evaluate total wall heat transfer, while the distribution of the heat transfer over the SRM particles is calculated using a stochastic approach, explained by Tuner [36] and further validated by Franken et al. [41] using Direct Numerical Simulation (DNS) results from Schmitt et al. [42]. A short overview of the turbulence models adopted in the present work is given in the following sub-section.

2.2. Phenomenological Turbulence Models and Particle Interaction

The expression of the mixing term in Equation (4) is presented below:

$$\left.\frac{\partial F_{\Phi}}{\partial t}\right|_{mix} = \frac{C_{\Phi}\beta}{\tau}\left[\int_{\Delta\psi} F_{\Phi}(\psi-\Delta\psi,t)F_{\Phi}(\psi+\Delta\psi,t)d(\Delta\psi) - F_{\Phi}(\psi,t)\right] \quad (5)$$

C_{Φ} and β are two model parameters that in the present study have been set to 2.0 and 1.0, respectively. The mixing time history, τ in Equation (5), is the main input parameter of the SRM. The mixing time is needed to model the turbulent mixing occurring in the combustion chamber due to various phenomena such as: fuel injection, swirl motion, tumble motion, etc. The shape and magnitude of the mixing time profile controls how intense the SRM particle mixing process is. Since τ influences mixture inhomogeneities in both composition and enthalpy spaces, a strong influence on the auto-ignition process, the local rates of heat release and pollutant formation are seen when the mixing time is changed.

A simple approach to construct the mixing time history is by using a set of empirical constants as done by Pasternak et al. [43,44] for Diesel combustion studies. A more comprehensive approach is to calculate τ during run-time by employing a k-ε or K-k based turbulence model. Depending on whether Diesel or gasoline combustion are considered, different approaches have been implemented in the present work. For Diesel combustion, the approach initially proposed by Kožuch [45] was adopted and validated by Franken et al. [46] across a large set of operating points. For gasoline engine conditions, the K-k model proposed by Dulbecco et al. [47] was implemented and validated in the SRM framework for different gasoline fuel surrogate mixtures in [48,49]. Examples of the mixing time histories that are computed with the mentioned turbulence models are shown in Figure 2 as function of crank angle degrees (CAD) assuming 0 as firing top dead center (TDCf).

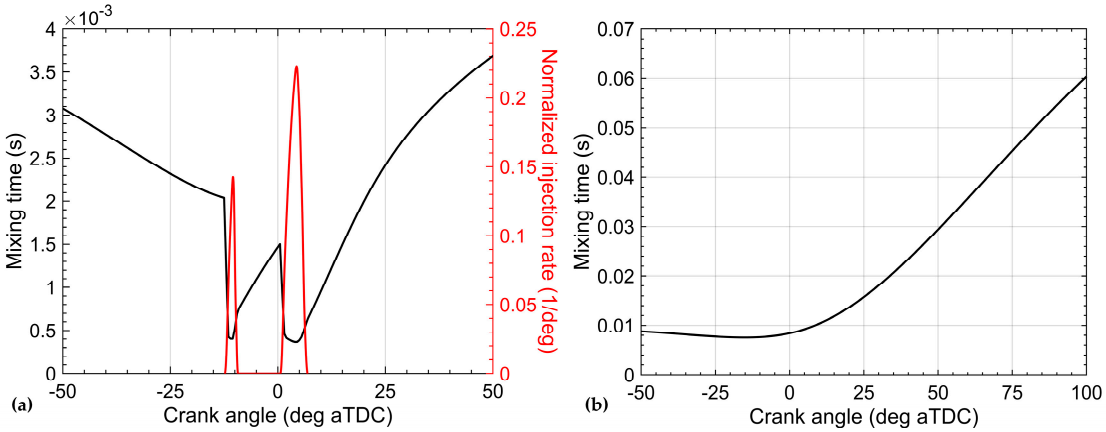

Figure 2. Exemplary mixing time histories computed using turbulence models for (**a**) Diesel engine conditions [47] and (**b**) gasoline engine conditions [49].

Once the mixing time history has been computed, an additional sub-model is employed to decide which and how many particles are selected in each mixing step. In this work the Curl model [50] has been used to describe the particle interaction for both the Diesel and the gasoline engine simulations.

2.3. Combustion Progress Variable Model

The CPV model relies on the pre-tabulation of the auto-ignition and emission formation processes for a broad range of initial conditions in terms of exhaust gas recirculation rates (yEGR), pressure (p), unburned temperature (T_u) and equivalence ratio (ϕ). The reconstruction of the thermo-chemical state during run-time is then performed by means of an appropriately chosen progress variable (herein noted as C). As discussed in detail by Niu et al. [51] and Ihme et al. [52], any progress variable-based method needs to fulfill the following conditions to be mathematically sound: (1) strict monotonicity with time; (2) non-negativity and normalization (C = 0 for unreacted mixture and C = 1 for fully burned mixture); (3) if reactive scalars (i.e., chemical species) are used in the definition of the progress variable, said scalars should evolve on comparable time scales [52].

Several progress variable definitions have been proposed by different groups for both homogeneous and flamelet-based tabulation frameworks [10,13,21]. The most common approach consists in formulating the progress variable via a combination of chemical species (typically including the surrogate fuel molecule, O_2, CO, CO_2, H_2O, OH, CH_2O and others). The choice of the species to use and their weighting factors within the progress variable definition is usually optimized so that both low and high temperature combustion regimes are captured [51,52]. In the present work, latent enthalpy (enthalpy of formation at standard state, h_{298}) is used to define the reaction progress variable C as reported below in a normalized fashion.

$$C(t) = \frac{h_{298}(t) - h_{298,u}}{h_{298,max} - h_{298,u}} \tag{6}$$

In Equation (6), h_{298} is the latent enthalpy calculated at 298 K, and summed over all species, subscript u denotes unburned state, and max denotes the most reacted state, which is assumed to be where the maximum of the accumulated chemical heat is released. As discussed in [15,33], this progress variable can be used to track both low and high temperature reactions, which is important when tabulation methods are developed for fuels exhibiting cool flames. Figure 3 shows an exemplary h_{298} profile together with temperature for a constant pressure reactor calculation.

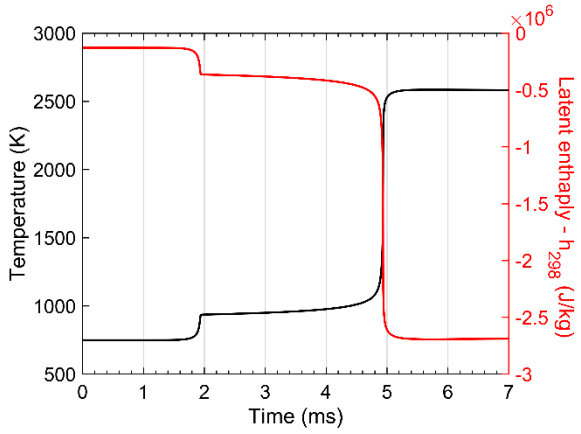

Figure 3. Temperature (black) and latent enthalpy at 298 K (red) as function of time for a constant pressure reactor calculation at 10 bar and 750 K for stochiometric *n*-heptane/air mixture.

It can be discussed that in a constant pressure reactor, progress variables based on temperature (i.e., as proposed by Knop et al. [24]) or on latent enthalpy will be equal. However, unlike temperature the latent enthalpy will not be influenced by pressure changes, fuel vaporization or mixing. As h_{298}

is a conserved scalar, a transport equation, as well as a spray source term, can be easily formulated. For the majority of the tabulated conditions, the maximum of the accumulated chemical heat release coincides with the chemical equilibrium state. However, for fuel-rich conditions as well as for states that lead to pronounced endothermic reactions (i.e., high pressure or high EGR conditions), the mixture relaxation towards equilibrium is not taken into account by Equation (6). Nevertheless, this definition was considered acceptable for engine applications in the SRM since it affects a small fraction of the particles for a limited portion of the cycle in direct injected-engine simulations. Over the whole range of computed conditions, this definition was found to be convenient to correctly capture both low and high temperature combustion regimes when generating the table through adiabatic homogeneous constant pressure reactor calculations. To keep the table size within a feasible range for engine applications, storage of the progress variable source terms was done over 25 points for each reactor simulation.

As introduced in [33], the coupling of the CPV solver with the SRM required substantial changes to the pre-existing online chemistry-based code. As discussed in the previous section, the tabulated chemistry solver requires only a reduced set of scalars as opposed to the full vector of species mass fraction needed for the online solver. It is important to notice that the normalized reaction progress, as reported in (6), is not transport directly. The latent enthalpy (h_{298}) is transported instead and the progress variable is calculated, whenever a table look-up is needed. This practice facilitates the formulation of the fuel injection model and the resulting evaporation source term and the particle–particle interaction sub-model. Beside the treatment of the chemistry step, the same set of sub-models noted in Equation (4) and their relative constants were applied for both the tabulated chemistry runs the online chemistry simulations. Hence potential differences between the two solver solutions are to be interpreted as due to the chemistry step only.

3. Look-Up Table Generation and Testing

Prior to the engine simulation campaigns, a grid density investigation together with an assessment of the interpolation error was performed so that the CPV model could be verified. In the following sub-sections, the details of the table construction process as well as the outcome of the interpolation error analysis are discussed.

3.1. Look-Up Table Generation

Detailed chemistry simulations under adiabatic constant pressure reactor conditions were performed using the software LOGEtable [53]. Initial mixture unburned temperature (T_u), pressure (p), equivalence ratio (ϕ) and mass fraction EGR (yEGR) are the input variables of the look-up table generator. Table grid points were chosen so that the typical range of thermodynamic conditions encountered in conventional direct injected engines that can be expected to be found in conventional direct injected engines. The table grid adopted in this work relies consists of 205,200 points which are distributed across tabulation parameters as outlined in Table 1.

Table 1. Tabulation grid adopted for all tabulated chemistry runs.

Parameter	Lower Bound	Upper Bound	Number of Points
Unburned Temperature (K)	300	1400	76
Pressure (bar)	1.0	200	18
Equivalence Ratio (-)	0.05	6.0	30
EGR mass fraction (-)	0.0	0.4	5

Except for the EGR mass fraction space, the points are distributed in a non-equidistant manner so that typical engine relevant conditions (i.e., around stoichiometry in equivalence ratio space) are better resolved. The EGR stream is assumed to have a fixed composition comprising combustion products (CO_2, H_2O and N_2) of the given fuel mixture at stoichiometry.

For each of the table grid points, the progress variable C introduced in Equation (6) is used to trace the reaction trajectory, and its source terms (dC/dt) are stored in the table at 25 different points between unburned C = 0 and fully burned C = 1.0 state. In addition, mean molecular weight, the thermodynamic polynomial coefficients and any chemical species that the user decides to monitor are also stored across the mentioned progress variable grid. In the present work, the following species have been included in the tabulation process so that major engine-out emissions and standard engine performance analyses could be done: fuel molecule, i.e., n-C_7H_{16}, O_2, N_2, CO_2, H_2O, CO, H_2, C_2H_2, C_2H_4 and unburned hydrocarbons (uHC) (defined as the sum of all species containing an H and C or H, C and O atoms). The resulting size on disk was approximately 1 GB.

3.2. Table Density/Accuracy Investigation

Before applying the CPV solver to engine simulations in the SRM, the interpolation strategy for the progress variable source term retrieval was verified. For each of the data entry points included in the tabulation grid (see Table 1), the auto-ignition solution from the constant pressure reactor calculation using the online chemistry solver has been compared to the respective solution retrieved from the table using linear interpolation. The discrepancy between the two solution has been quantified based on the mean relative difference of the vector composed by the errors at 5, 10, 50 and 90 percent of energy released location (noted as $E_{5\%}$, $E_{10\%}$, $E_{50\%}$ and $E_{90\%}$ in Figure 4) at all given reactor points.

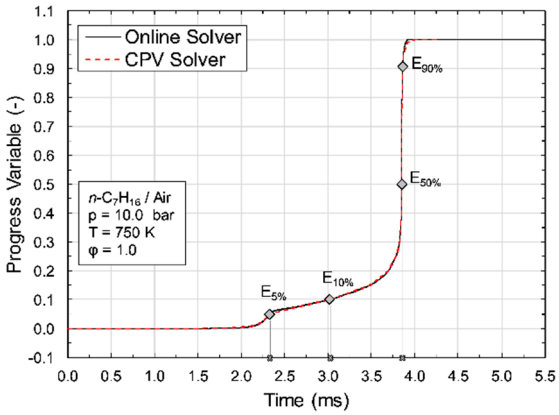

Figure 4. Online and tabulated chemistry solutions for the progress variable (based on Equation (6)) evolution of a stoichiometric *n*-heptane/air mixture at 10 bar and 750 K.

The global interpolation error has been then defined based on the mean square difference (MSD) of the location of $E_{5\%}$, $E_{10\%}$, $E_{50\%}$ and $E_{90\%}$ points. In Equations (7), where i = 5, 10, 50, 90, the exact definition of the interpolation error is reported.

$$\varepsilon_i = \frac{E_{i,Tabulated} - E_{i,Online}}{E_{i,Online}} \times 100\,\overline{\varepsilon} = \sum_{i=1}^{N_{errors}} |\varepsilon_i| / N_{errors}\,\varepsilon_{MSD} = \sqrt{\sum_i (\overline{\varepsilon} - |\varepsilon_i|)^2} \quad (7)$$

The interpolation errors have been assessed for a large set of operating conditions covering lean to rich (ϕ = 0.6–3.0) conditions as well as from low to high unburned temperatures (T = 600–1400 K) under constant pressure reactor conditions. *n*-Heptane was used as fuel molecule, and the mechanism developed by Zeuch et al. [54] was employed. The main goal of this campaign was to quantify the accuracy of the interpolation routine under the simplest reactor conditions, so to have a higher confidence in results assessment during the subsequent engine simulation campaign. In the SRM simulation, numerous sub-models are coming into play, and hence, error compensation effects may arise. In Figure 5, exemplary results of the error quantification campaign are displayed in pixel plot format for conditions at 1 and 35 bar pressure.

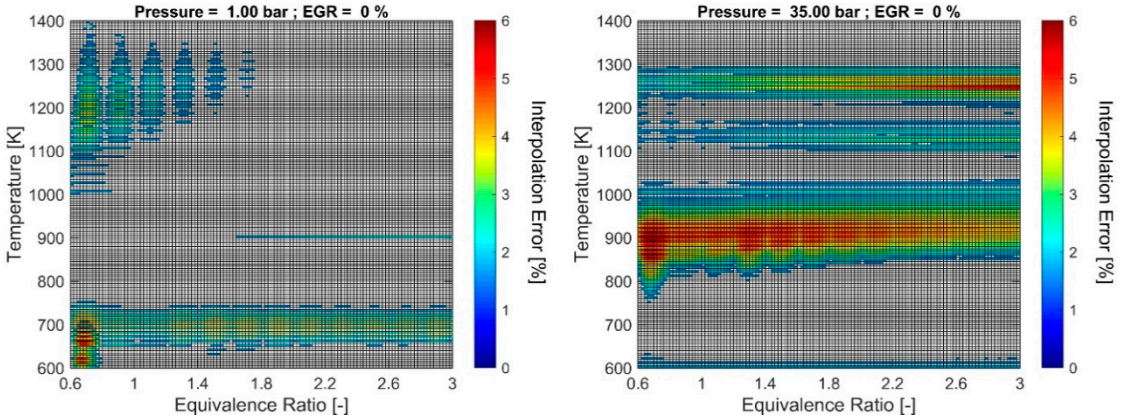

Figure 5. Error maps for the interpolation error (ε_{MSD} as defined in Equation (7)) between online and tabulated chemistry solver under constant pressure reactor conditions (**a**) at 1 bar and (**b**) 35 bar, both at 0% exhaust gas recirculation using *n*-heptane as fuel.

For a more effective error visualization as well as to better highlight the exact areas where interpolation errors may arise, pixel contours have been conditionally formatted so that every case having an error below 0.5% is displayed in white. All cases presenting an error above 0.5% will have contours consistent with the RGB color bar instead. For the whole range of computed conditions, the solution retrieved from the table did not exceed a 6% discrepancy on a single point basis, while the overall average error is approximately 1.5%. As expected, interpolation errors are more visible in the Negative Temperature Coefficient (NTC) regimes, which is the most challenging area to parametrize when progress variable methods are concerned [24,55]. While a tighter tabulation grid in temperature space could have delivered even lower errors, the authors considered this level of accuracy to be acceptable. This decision was based on the globally low errors but also on method usability considerations.

A tighter table grid results in a larger file size on disk, which in turn affects the random-access memory (RAM) requirement for the engine simulations during run-time. Hence, the present configuration was considered to be a good trade-off.

4. Compression Ignition Engine Simulations

In this section, results of a heavy-duty Diesel engine simulation campaign are presented and discussed. In the first sub-section, experimental data and simulation setups are presented. Secondly, a result comparison between experimental data and the two chemistry solvers is shown and discussed with respect to engine performance parameters and engine-out emissions. All the simulation results presented in this section were obtained using the commercial software LOGEengine version 3.2.1 [53].

4.1. Engine Data and Simulation Setup

The simulation setups were constructed based on experimental data from a heavy-duty (HD) 13.0 L Diesel engine that features a direct injection system capable of injection pressures up to 2000bar. Although the engine has an in-built external EGR system, the analyzed engine conditions did not include external EGR. A total of 10 operating points from 1000 rpm to 1700 rpm and 6 bar to 22 bar indicated mean effective pressure (IMEP) are used for the present simulation campaign. Details of the operating conditions are outlined in Table 2.

Table 2. Heavy-duty engine operating conditions.

Case Name	Speed (rpm)	IMEP (bar)	EGR (mass%)	Injection Pulses (#)
HD01	1700	19.0	4.0	1
HD02	1300	22.0	4.0	1
HD03	1300	14.5	4.0	1
HD04	1300	6.0	4.0	1
HD05	1200	6.0	4.0	1
HD06	1200	14.5	4.0	1
HD07	1200	22.0	4.0	1
HD08	1000	6.0	4.0	1
HD09	1000	11.0	4.0	1
HD10	1000	22.0	4.0	2

As presented in Figure 6, operating point 10 features a double injection rate profile (pilot + main) while the rest have a single injection event. The crank-angle resolved pressure profiles were measured for one cylinder and used to calibrate the SRM engine model.

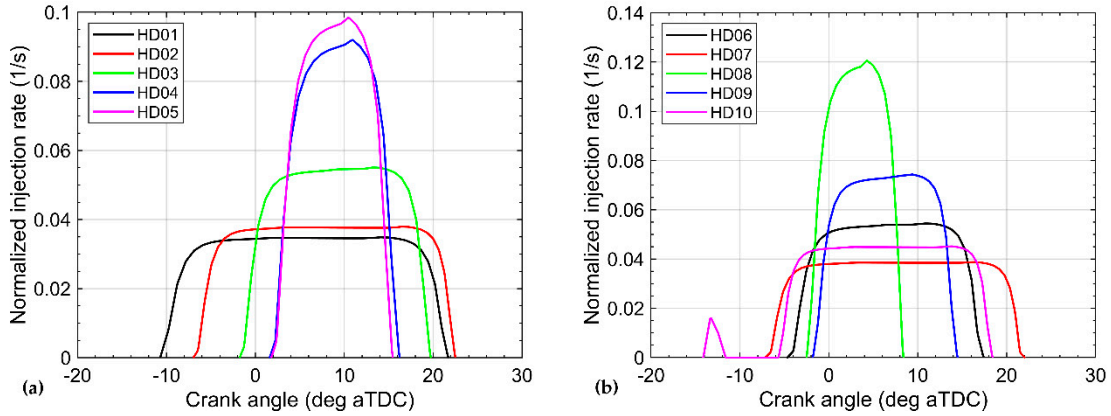

Figure 6. Fuel injection rates as a function of crank angle degree (assuming 0 as firing TDC) for operating conditions (**a**) from 1–5 and (**b**) 6–10, as listed in Table 2.

Commercial Diesel fuel was used during experiments, whereas in the simulations a blend of *n*-decane and *α*-methylnaphthalene (75–25% mass fractions respectively, also noted as IDEA surrogate fuel) was employed as surrogate fuel model. A liquid fuel properties comparison is summarized in Table 3.

Table 3. Liquid properties of the experimental and surrogate fuel mixture used in the heavy-duty Diesel engine simulation campaign.

Fuel Name	Lower Heating Value (MJ/kg)	Density at 15 °C (kg/m^3)	Cetane Number (-)	C (w%)	H (w%)	O (w%)
EU Diesel	41.6	820.0	49	86.0	13.4	0.6
IDEA surrogate fuel	42.94	783.0	52.3	86.62	13.38	0.0

The chemical kinetic scheme employed in this study has been taken from the LOGEfuel database [53]. The mechanism is an improved version of the detailed model from Wang [56]. It features oxidation models for *n*-decane, *α*-methyl-naphthalene and methyl decanoate as main fuel species as well as a detailed PAH growth mechanism [57] and thermal NO_x model. The detailed reaction scheme was reduced to a size of 189 species using the method described in [12].

The measured pressure history was analyzed using the thermodynamic analysis of LOGEengine [53]. This procedure provided chemical kinetics-based estimations of wall temperature,

in-cylinder temperature at IVC, internal EGR fraction and the apparent rate of heat release (RoHR). In Tables 4 and 5, the main SRM model parameters and the calibrated k-ε model constants are presented, respectively [45].

Table 4. SRM main model settings for the heavy-duty Diesel engine simulation campaign.

Parameter	Value
Number of particles (-)	500
Simulation time-step (CAD)	0.5
Number of consecutive cycles (-)	30
Woschni constant C1	2.28
Woschni constant C2	0.0035
Stochastic heat transfer constant (-)	15

Table 5. Calibrated constants for the k-ε turbulence model.

C_{squish}	$C_{injection}$	C_{swirl}	$C_{dissipation}$	C_{tau}
1.0	11.0	136.0	9.1	0.35

The SRM model calibration for the presented operating conditions was carried out using the procedure described in [58], and the Curl [50] particle interaction sub-model was used. To ensure consistency during chemistry solver comparisons, the same set of model parameters and constants were applied to both the online and tabulated chemistry solver runs without any re-calibration.

4.2. Simulation Results

In Figure 7, comparisons of experimental and simulated in-cylinder pressure histories, rate of heat release, combustion phasing parameters and normalized emissions are presented for a low-load (HD04), a mid-load (HD06) and a high-load (HD07) operating points. The quantities noted in the following figures as CA05, CA10, CA50 and CA90 represent the crank angle location at which 5, 10, 50 and 90 per cent of the total heat has been released, respectively.

Detailed comparisons by means of pressure, RoHR and crank angle resolved emissions for all the operating conditions listed in Table 2 can be found in Appendix A. In Figure 8, comparisons of the CA50, peak cylinder pressure location in CAD (PCP_{CAD}), as well as CO, CO_2, unburned hydrocarbons (uHC) and NO at EVO are shown for all operating points. To comply with data confidentiality restrictions, all the results shown in this simulation campaign are presented in a normalized fashion. With respect to engine out emissions, different normalization strategies have been applied to ensure meaningfulness of the shown comparisons. More in detail, for CO_2 and NO, the simulated ppm values have been normalized with respect to the experimental measurements. For CO and uHC instead, the normalization has been computed based on the difference in ppm between simulated and experimental data with a threshold value set to approximately 100 ppm. In other words, if simulated uHC or CO presents a normalized factor of 2.0, it means that the absolute difference between experimental and simulated values is approximately 200 ppm.

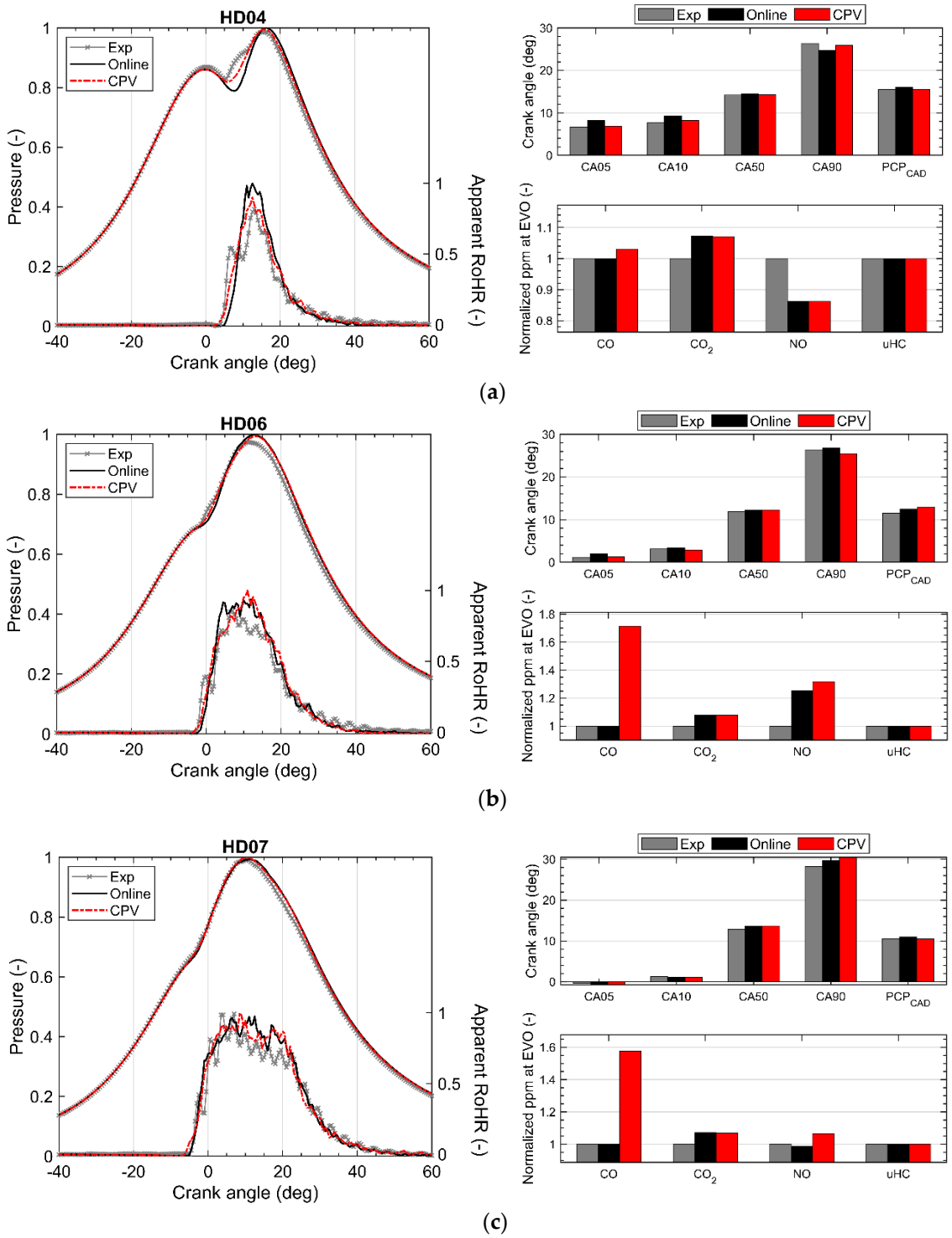

Figure 7. In-cylinder pressure history and apparent rate of heat release (left), combustion phasing parameters (top right) and normalized engine-out emissions (bottom right) comparisons between experimental data and SRM simulations for operating points (**a**) HD04, (**b**) HD06 and (**c**) HD07.

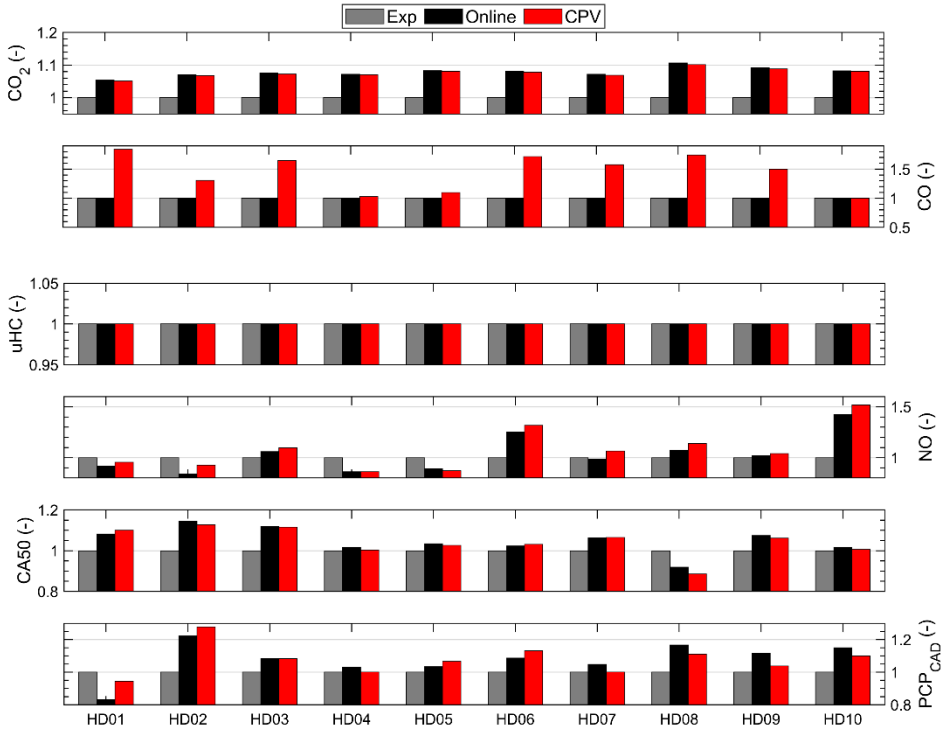

Figure 8. Experimental and simulated engine-out emissions as well as performance parameters (CA50 and PCP_{CAD} location) for all operating conditions of the heavy-duty engine simulation campaign. Data have been normalized with respect to experimental values.

On the other hand, if simulated and experimental HC or CO differ by less than 100 ppm, then the factor is set to 1.0, so to underline an acceptable agreement. Such formulation was considered necessary to cope with the fact that the measured CO and uHC are in absolute terms very low. Hence a standard normalization would have resulted in a set of misleadingly high factors for CO and uHC from the engineering standpoint. For uHC, in particular, the difference between experimental and simulated engine-out ppm values never exceeded 30 ppm across all the operating points, and therefore, the set of comparison factors for uHC in Figure 8 is homogeneously set to 1.0.

By means of combustion phasing, the SRM results are in good agreement with experimental data for the majority of the analyzed operating conditions. Visible discrepancies can be observed by means of peak cylinder pressure predictions in HD08 and HD09. However, such result was considered acceptable, considering that on the experimental side, these operating points showed a strong cycle-to-cycle variability, as it can be noticed via the large fluctuations of the heat release rate between 0 and 40 crank angle degrees after TDC (see Figures A8 and A9 in Appendix A).

As for the online versus CPV simulation results, both simulations resulted to be in close agreement with each other across the whole range of simulated data. The tabulated chemistry solver predicted a combustion phasing within less than 0.5 CAD difference with the detailed online chemistry solver at the mid and high loads. For the low load points (HD04 and HD05), a slightly more noticeable difference (≈2.0 CAD) between online and tabulated chemistry solutions can be seen when comparing the predicted start of combustion (See Figures A4 and A5 in Appendix A). At low loads, combustion initiates while the mixture is the NTC region, which, as discussed in Section 3.2, is the most challenging regime for progress-variable-based models. It is therefore likely to happen that under these conditions the interpolation error starts to play a visible role. Nevertheless, a 2 CAD discrepancy in start of combustion is well within a range typically considered acceptable for engine performance studies and considering accuracy of the sensors used during the experimental campaigns.

With respect to engine-out emissions, both solvers showed good agreement with experimental data for CO_2, uHC and NO. Differences in CO_2 are explained by differences in the C/H ratio of the real fuel blend and the surrogated fuel blend. These differences also influence the CO emission calculation. With respect to NO, the differences between tabulated and detailed chemistry are lower than differences between the SRM predictions and the engine measurements. For these species, it can be stated that the accuracy of the tabulated chemistry solver is not influencing the accuracy of the tool chain. This statement is also true for the prediction of CA50 and PCP. For carbon monoxide emissions, the online chemistry solver showed a noticeably closer match (less than 100 ppm difference) with experimental data. While the CO predictions from the CPV solver lie within a more than acceptable range from the engineering point of view, it is important to note that correct tabulation of CO during the expansion phase is another challenging area when progress variable models are concerned. Unlike methods proposed in [23,24], the present method does not account for a time-scale dependent retrieval of the CO emissions from the table. This means that the accuracy of the final CO yield depends on how the close to (or far from) equilibrium the value stored in the table at progress 1 is. In the present study, the presented level of accuracy between online and tabulated chemistry solver-based CO values (± 200 ppm) was considered to be acceptable. In future studies, however, a time-scale dependent CO retrieval strategy will be considered.

5. Gasoline Engine Simulations

In this section, results of a spark-ignited engine simulation campaign are shown and discussed. In the first sub-section, a brief description of the experimental data and computational setups are presented. Secondly, engine performance parameters and engine-out emissions are compared between experimental data, online and tabulated chemistry solver. All the simulation results presented in this section were obtained using the commercial software LOGEengine version 3.2.1 [53].

5.1. Engine Data and Simulation Setups

The experimental data were measured on a single cylinder research engine at the TU Berlin [48]. Cylinder bore and stroke are 82.0 and 71.9 mm, respectively, while the compression ratio is 10.75:1. The single cylinder engine is specifically designed for combustion investigations and features both port and direct fuel injection systems. The present engine experiments were conducted using the centrally mounted direct fuel injector. The start of fuel injection is at −270 CAD aTDC. Eight fired operating points were selected and are summarized in Table 6. For each operating condition, in-cylinder as well as manifold pressure were recorded for 250 consecutive cycles by means of a low- and high-pressure sensors. More details on the experimental setup and measuring equipment used can be found in Kauf et al. [59].

Table 6. Spark-ignition engine operating conditions.

Case Name	Speed (rpm)	IMEP (bar)	EGR (mass%)	Spark timing (CAD aTDC)
SI01	1500	15.0	1.7	−1.5
SI02	2000	5.0	9.1	−4.0
SI03	2000	10.0	4.9	−6.0
SI04	2000	15.0	2.0	−3.0
SI05	2000	20.0	1.1	2.0
SI06	2500	5.0	9.4	−9.0
SI07	2500	10.0	4.9	−5.0
SI08	2500	15.0	2.0	−5.0

The fuel used during the experimental campaign was a RON95 E10 commercial gasoline, at 150 bar injection pressure. A four-component mixture comprising mole percentages of 31.9% *iso*-octane, 11.4% *n*-heptane 35.6% toluene and 20.8% Ethanol was used in the simulation campaign instead. Comparisons of the major fuel properties are listed in Table 7. The adopted reaction mechanism is

based on the detailed ETRF scheme developed by Seidel consisting of 475 species and 5160 reactions. The detailed reaction scheme was validated for different experiments and engine relevant conditions for both auto-ignition and laminar flame speed in several previous works [39,60].

Table 7. Liquid properties of the experimental and surrogate fuel mixture used in the SI engine simulation campaign.

Fuel Name	Lower Heating Value (MJ/kg)	Density at 15 °C (kg/m^3)	RON/MON (-)	C (*n*)	H (*n*)	O (*n*)
E10 Gasoline	41.78	748.7	96.7/85.8	6.6	12.8	0.21
ETRF mixture	41.14	756.4.0	96.7/87.4	6.3	11.8	0.21

The SRM model calibration for the presented operating conditions was carried out using the procedure described in [61]. In Tables 8 and 9, the main SRM model parameters and the calibrated K-k model constants [47] are presented, respectively. As done for the compression ignition engine campaign, the same set of model parameters and constants were applied to both the online and tabulated chemistry solver runs without any re-calibration.

Table 8. SRM main model settings for the spark-ignition engine simulation campaign.

Parameter	Value
Number of particles (-)	500
Simulation time-step (CAD)	0.5
Number of consecutive cycles (-)	30
Woschni constant C1	2.28
Woschni constant C2	0.0035
Stochastic heat transfer constant (-)	15

Table 9. Calibrated constants for the K-k turbulence model.

$C_{injection}$	$C_{compression}$	$C_{dissipation}$	C_{TKE}	C_{length}	C_{β}	$C_{\Delta,1}$	$C_{\Delta,2}$	C_{tau}
0.005	0.67	1.0	0.85	0.30	0.25	0.073	0.1313	4.3

5.2. Simulation Results

In Figure 9, comparisons of experimental and simulated in-cylinder pressure histories, rate of heat release, combustion phasing parameters and normalized emissions are presented for a low-speed mid-load (SI01), a mid-speed high-load (SI05) and a high-speed low-load (SI06) operating points. Extended comparisons by means of pressure, RoHR and crank angle resolved emissions for all the operating conditions listed in Table 6 can be found in Appendix B. Overall, the SRM simulation results show a close match with experiment by means of in-cylinder pressure for different operating conditions. Slight deviations can be seen for the operating points SI05 (2000 rpm and 20 bar IMEP) and SI06 (2500 rpm and 5 bar IMEP) in Figure 9b,c by means of start of combustion and peak cylinder pressure. However, the overall agreement is considered to be acceptable, especially considering the typical cycle-to-cycle variability. Compared to the Diesel engine campaign, a much closer match between online and CPV solver can be seen in the SI cases.

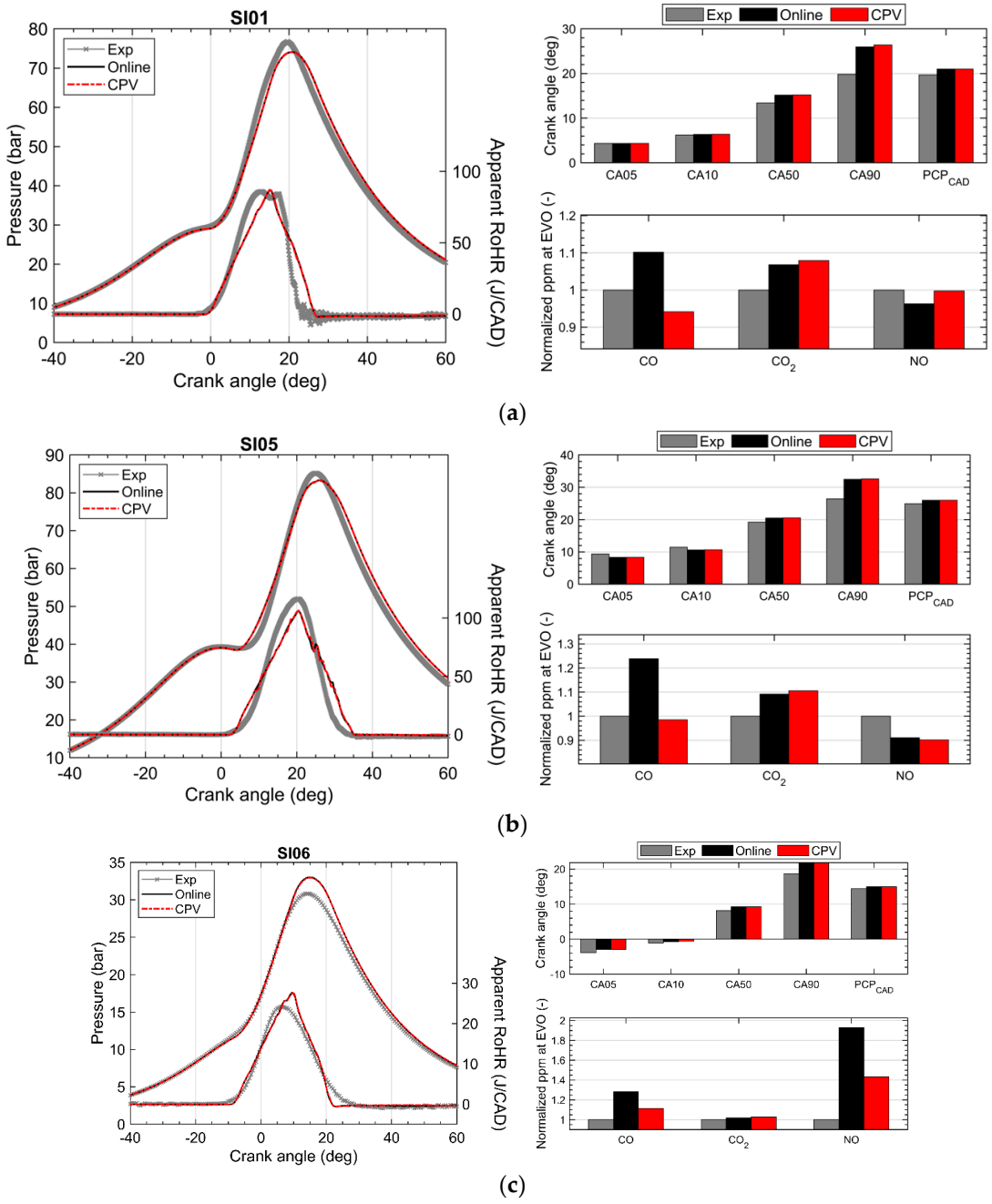

Figure 9. In-cylinder pressure history and apparent rate of heat release (left), combustion phasing parameters (top right) and normalized engine-out emissions (bottom right) comparisons between experimental data and SRM simulations for operating points SI01 (**a**), SI05 (**b**) and SI06 (**c**).

This is explained by the fact that in SI mode, the dominant phenomenon is the flame propagation rather than mixing controlled combustion, where particles reach fully burned state (C = 1) much faster and are moved to the burned zone. In addition, given the early start of injection, the mixture is assumed to be homogeneous and close to stoichiometry. The homogeneity in lambda, together with the particles quickly reaching C = 1, makes the interpolation particularly accurate. Stochastic effects are still present due to the SRM treatment of the heat transfer; however, hardly any difference can be seen in terms of pressure and rate of heat release histories as well as in terms of combustion phasing parameters and peak cylinder pressure location.

In Figure 10, engine-out emissions and major combustion phasing parameters are summarized for all the investigated operating conditions. All values are normalized to experimental data. By means of engine-out emissions, while simulations and experiments agree acceptably well, for most of the cases, noticeable differences can be seen for CO and NO between online and tabulated chemistry solver. Regarding NO, the differences are related to the fact that in the detailed scheme a more advanced prompt and thermal formation mechanism for NOx is accounted for, while in the tabulated chemistry solver only thermal NO source terms are considered. As for CO, a similar discrepancy as in the Diesel simulation campaign can be seen. The operating point SI06 (at 2500 rpm and 2 bar IMEP) shows the largest difference (approximately 17%) for NO emissions against experimental data. This may be explained by the noticeable in predicted peak cylinder pressure which results in a different in-cylinder temperature. The comparison of the tool chain accuracy and the tabulated chemistry solver accuracy is leading to similar conclusions as for the Diesel engine test case in Section 4.

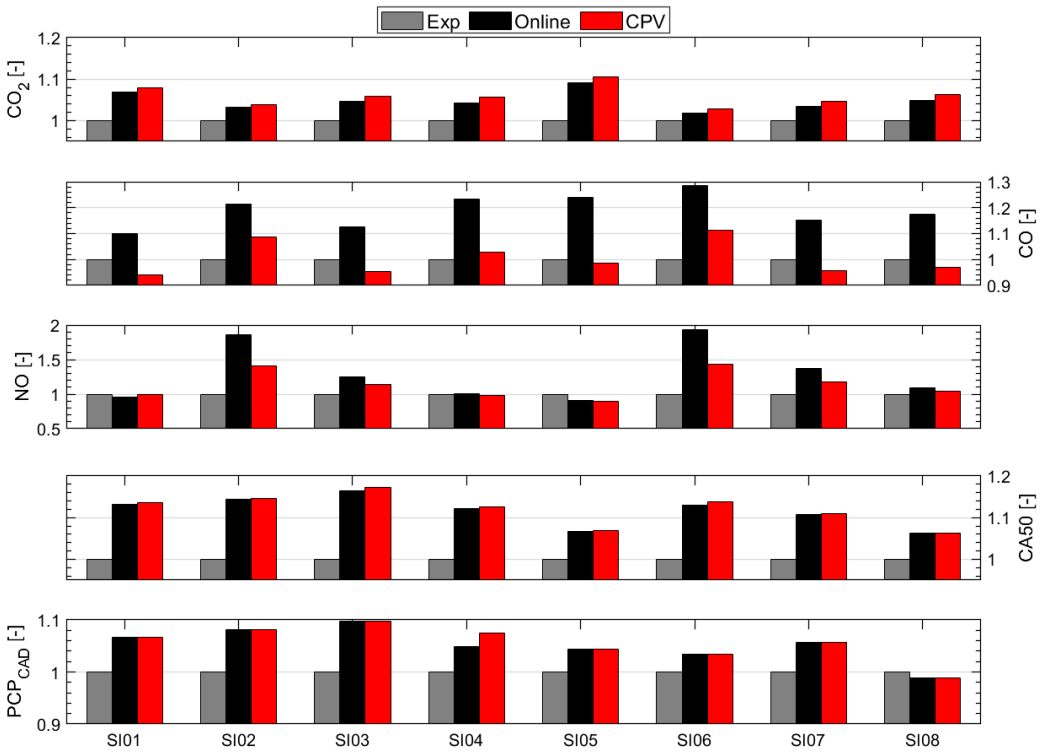

Figure 10. Experimental and simulated engine-out emissions as well as performance parameters (CA50 and PCP_{CAD} location) for all operating conditions of the SI engine simulation campaign. Data have been normalized with respect to experimental values.

6. Computational Aspects

With respect to the SI engine campaign (see model settings in Table 8), a single SRM cycle simulation employing the 475 species chemical mechanism using the online chemistry solver takes approximately 19 min to complete on 24 parallel cores (Intel Xeon E5-2687W v4 @ 3.00GHz processors from the year 2016). The simulation of thirty consecutive cycles results in a total CPU time per operating point of 9.4 h. Although these figures are a small fraction of the CPU cost of a RANS 3-D CFD multi-cycle simulation, typical 0-D/1-D simulation frameworks (i.e., based on a multi-zone Vibe combustion model) usually require a few tenths of a second to run and, in some cases (i.e., Mean Value Engine Models MVEMs), real-time simulation capability is easily reached. In addition, considering that the turbulence model calibration procedure [49,58] relies on a few thousands of Genetic Algorithm (GA) driven SRM simulations to find the optimal constants (see Tables 5 and 9), the application of the online chemistry solver with large mechanisms (i.e., more than 150 species) becomes unfeasible

for engine development studies such as driving cycle simulations or engine performance mapping. With respect to the present simulation campaigns, a summary of the CPU times obtained with both solvers and the reported model settings (see Tables 4 and 8) are reported in Table 10.

Table 10. Computational performance summary assuming SRM model settings listed in Tables 4 and 8, on an Intel Xeon E5-2687W v4 @ 3.00GHz CPU from the year 2016.

Simulation Setup	Online Chemistry on 24 Parallel Cores (s/cycle)	Tabulated Chemistry on 1 Core (s/cycle)
SI engine simulation	1136.5	4.1
CI engine simulation	631.7	1.6

Considering that the SRM with CPV tabulated chemistry solver can be easily run on a single core, as opposed to the online chemistry solver that requires multiple cores per run, one can conclude that the present solver delivers a speed-up of at least three orders of magnitude. The size of the auto-ignition table valid for a wide range of typical engine relevant conditions including EGR variations (between 0 and 40%) requires about 1.0 GB of RAM memory. These level resource requirements allow usage of the SRM with CPV not only on dedicated high-performance computing (HPC) systems but also on modern industry grade laptops. Moreover, given the high degree of physical and chemistry models included in its formulation, engine parameter optimization campaigns can be performed within feasible engineering times. To put the computational results shown in Table 10 in a broader prospective, in Figure 11 are shown the extrapolated computational costs of two relevant engine development simulation campaigns: an engine performance mapping and a WLTP cycle.

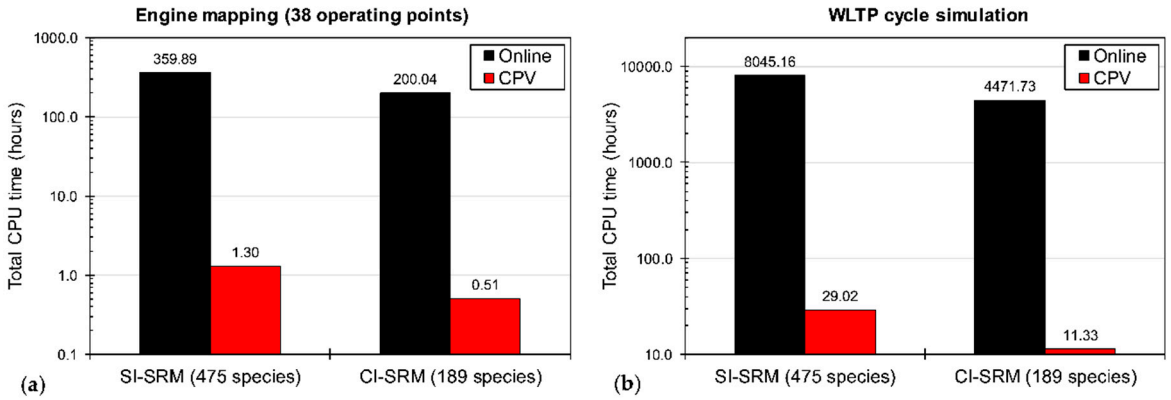

Figure 11. Comparison between online and tabulated chemistry solver computational performances for (**a**) a full engine performance mapping simulation campaign comprising a total of 38 operating conditions and (**b**) the simulation of the full WLTP cycle (30 min) in terms of combustion and emission simulations only.

Both results have been extrapolated considering only the CPU time needed by in-cylinder combustion model. Additional system components (i.e., intake and exhaust air paths, aftertreatment systems) and their contribution to the total simulation time are not considered. Nevertheless, it can be stated that the tabulated chemistry allows to include detailed chemistry effects in a number of applications that are, in most cases, unfeasible for the online chemistry solver.

The developed CPV tabulated chemistry solver was recently applied in two publications for the engine and fuel co-optimization of Diesel and gasoline engines. In the work of Franken et al. [58] a heavy-duty Diesel engine was optimized to find the best set of engine parameters to reduce fuel consumption and NO_x emissions at different speeds and loads. The authors reported optimization times of 20 h to 40 h for one operating point. For a single-cylinder, research on gasoline engine optimization campaign was published by Franken and co-authors [48,61]. A dual fuel tabulated

chemistry approach, based on CPV, was used to find the best set of engine parameters in terms of water/fuel-ratios to reduce the knock tendency at a high load operating point and improve the engine efficiency. The optimization times reported in [48,61] are within 10h for one operating point using 4 cores (Intel i7-7820HQ @ 2.90 GHz, from the year 2017) while an equivalent run with the online chemistry solver would have taken several days.

7. Conclusions

This article reported on the application and comparisons of two different chemistry solvers for in-cylinder combustion simulations of compression and spark-ignited engines using a zero-dimensional PDF-based framework. A well-stirred reactor-based online chemistry solver was compared to the developed progress-variable-based solver noted as CPV. Latent enthalpy is chosen as the only parameter for the formulation of the reaction progress variable while a dedicated source term-based method is applied to thermal NO formation. Verification of the newly introduced CPV solver was first assessed under homogeneous constant pressure reactor conditions in order to optimize the table density/interpolation accuracy trade-off. Subsequently, a stochastic reactor model was used to validate the interaction of chemistry and flow during engine combustion processes. Model performance with respect to experimental data and the two solvers was assessed under heavy-duty Diesel engine as well as passenger-car SI engine conditions.

The SRM was shown to be capable of predicting the mixing controlled as well as flame propagation driven combustion processes independently of the chemistry solver. Main engine-out emissions (CO, CO_2, NO and uHC) as well as combustion phasing parameters (CA50, PCP location) are in good agreement with experimental data. With respect to the results obtained with the online and tabulated chemistry solvers, minor differences have been noticed for the start of combustion location and CO emissions. Although still limited to a magnitude of 2.0 CAD, more noticeable discrepancies between the two solvers, in terms of combustion onset, were seen at low-load low-speed in both the Diesel and the gasoline engine simulation campaigns. Under these conditions, the fuel undergoes the NTC behavior where the interpolation error becomes more evident due to highly non-linear reactivity trajectories of the reacting mixture. Despite the thorough table grid optimization study performed to minimize interpolation error, when low temperature combustion is the dominant phenomenon, a tighter, if not adaptive, tabulation grid point distribution may be needed to match even better the start of combustion location predicted by the online chemistry solver. Nevertheless, given the accuracy level shown in the present work, it was concluded that the predictive capabilities of the 0-D SRM is well within commonly noted uncertainty ranges caused by, for instance, sensors inaccuracy or cycle-to-cycle variability.

From the computational cost standpoint, the CPV solver was found to be at least three orders of magnitude faster than the online chemistry solver while keeping the same order of chemical and physical models. The proposed approach is therefore a competitive tool, in terms of CPU time, to lower order methods (i.e., multizone Vibe models) widely used in 0-D/1-D engine performance studies. Generally, CPU cost is one of the main burdens when deployment of detailed chemical mechanisms in 0-D and 3-D CFD simulations is concerned. In particular, if simulations aim to an accurate prediction of exhaust emissions, it often comes a point where a trade-off has to be made between computational performances and size of the chemical mechanisms. Employing a tabulated chemistry solver has the potential to break this tread-off, by using the large mechanism only during table generation (a one-time process) while keeping the high-fidelity combustion and emission predictive capability. In conclusion, it can be stated that the present validation of CPV tabulated chemistry solver allows the SRM to be a useful CAE tool, which holds the accuracy of the overall model tool chain.

Author Contributions: Conceptualization, A.M. and T.F.; methodology, A.M., T.F. and L.C.G.M. Gonzales Mestre.; software, A.M., A.B. and T.F.; validation, A.M., T.F. and L.C.G.M. Gonzales Mestre.; formal analysis, A.M., T.F. and F.M.; investigation, A.M. and T.F.; resources, A.M.; data curation, A.M. and T.F.; writing—original draft preparation, A.M.; writing—review and editing, A.M. and T.F.; visualization, A.M.; supervision, A.B. and F.M.; project administration, A.M.; funding acquisition, A.M. All authors have read and agreed to the published version of the manuscript.

Funding: The research leading to these results has received funding from the People Programme (Marie Curie Actions) of the European Union's Seventh Framework Programme FP7/2007-2013/under REA grant agreement n° 607214. Funding from the Swedish Energy Agency (P39368-2-F-Flex2) is gratefully acknowledged.

Conflicts of Interest: The authors declare no conflict of interest.

Nomenclature

0-D	Zero-Dimensional
3-D	Three-Dimensional
AMN/1-MN	Alpha Methylnaphthalene, $C_{11}H_{10}$
aTDC	After Top Dead Centre
BEV	Battery Electric Vehicle
bTDC	Before Top Dead Centre
CAE	Computer Aided Engineering
CAD	Crank Angle Degree
CFD	Computational Fluid Dynamics
CFM1D-TC	One-Dimensional Coherent Flame Model-Tabulated Chemistry
CI	Compression Ignition
CMC	Conditional Moment Closure
CO	Carbon Monoxide
CO_2	Carbon Dioxide
CPV	Combustion Progress Variable
DI	Direct Injection
ECFM-3Z	Extended Coherent Flame Model 3 Zones
EGR	Exhaust Gas Recirculation
EOI	End of Injection
FPI	Flame Prolongation of Intrinsic Low Dimensional Manifold
ETRF	Ethanol Toluene Reference Fuel
GHG	Green House Gases
HCCI	Homogeneous Charge Compression Ignition
ICE	Internal Combustion Engine
ICEV	Internal Combustion Engine Vehicles
IFP-EN	French Institute of Petroleum
ILDM	Intrinsic Low Dimensional Manifold
KLSA	Knock Limit Spark Advance
LES	Large Eddy Simulation
LHV	Lower Heating Value
MD	Methyl Decanoate, $C_{11}H_{22}O_2$
MDF	Mass Density Function
NOx	Nitrogen Oxides
NTC	Negative Temperature Coefficient
OEM	Original Equipment Manufacturer
PAH	Polycyclic Aromatic Hydrocarbons
PaSR	Partially Stirred Reactor
RDE	Real Driving Emissions
RoHR	Rate of Heat Release
RANS	Reynolds Averaged Navier Stokes
SI	Spark Ignition
SOI	Start of Injection
SRM	Stochastic Reactor Model

TCI	Turbulence Chemistry Interaction
TKI	Tabulated Kinetics of Ignition
TDC	Top Dead Centre
TRF	Toluene Reference Fuel
uHC	Unburned Hydrocarbons
WLTP	Worldwide harmonized Light vehicle Test Procedure
WSR	Well Stirred Reactor

Appendix A Heavy-Duty Diesel Engine Simulation Campaign

In this section, in-cylinder pressure, apparent rate of heat release as well as CO, CO_2, uHC and NO profiles comparisons between experiments and simulations for both solvers are presented for all heavy-duty Diesel engine conditions outlined in Table 2.

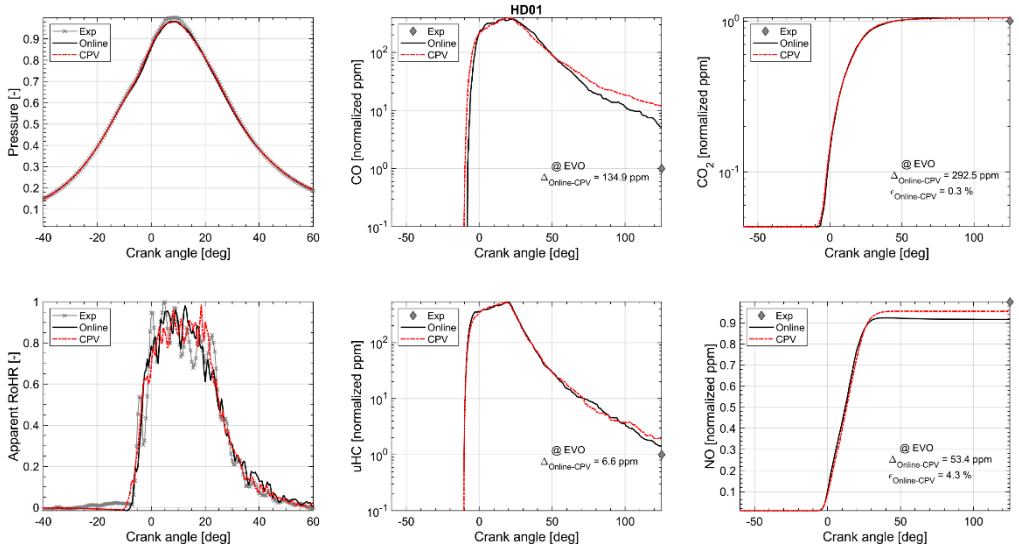

Figure A1. Engine performance and emissions for operating point HD01 (1700 rpm, 19.0 bar IMEP).

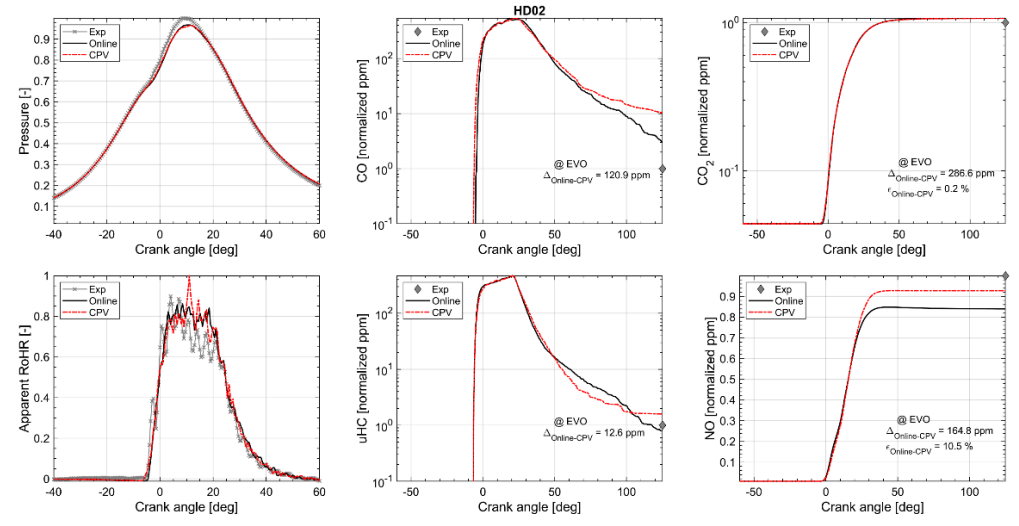

Figure A2. Engine performance and emissions for operating point HD02 (1300 rpm, 22.0 bar IMEP).

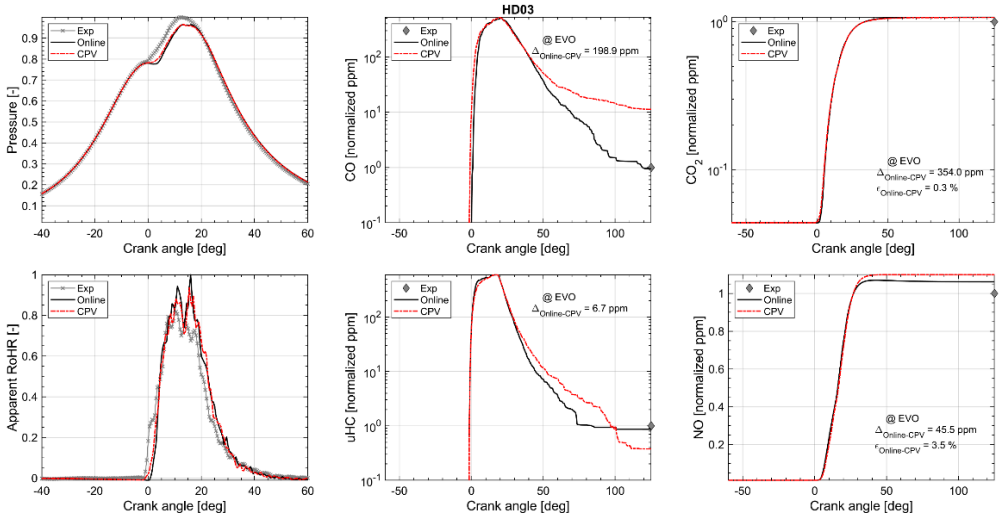

Figure A3. Engine performance and emissions for operating point HD03 (1300 rpm, 14.5 bar IMEP).

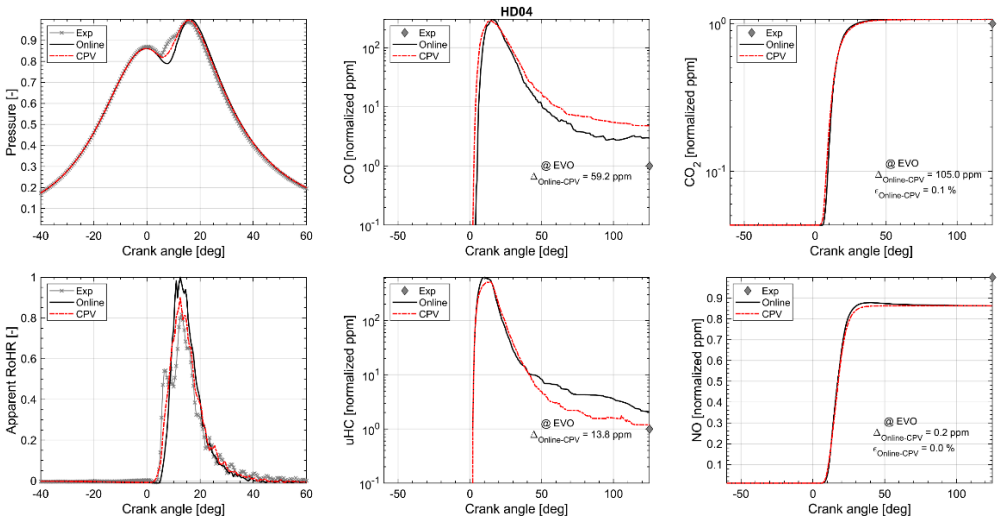

Figure A4. Engine performance and emissions for operating point HD04 (1300 rpm, 6.0 bar IMEP).

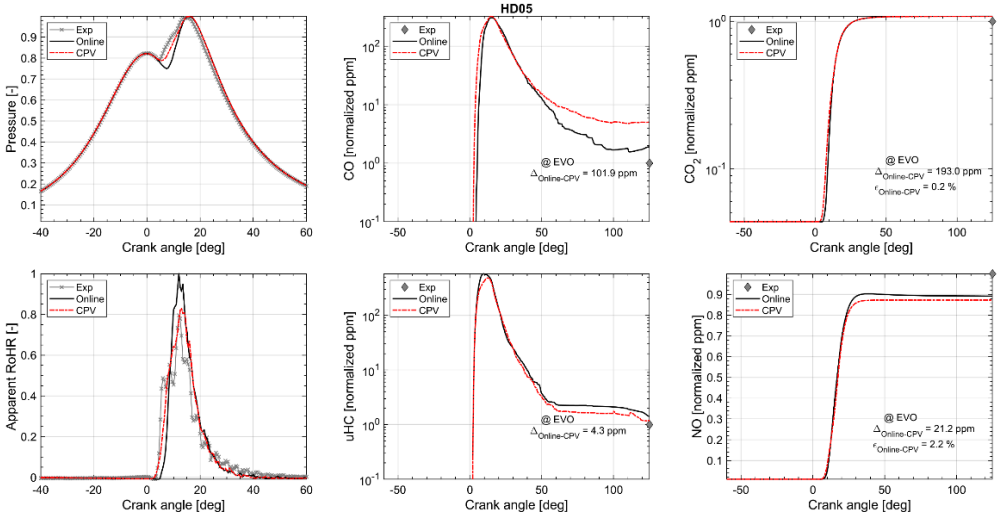

Figure A5. Engine performance and emissions for operating point HD05 (1200 rpm, 6.0 bar IMEP).

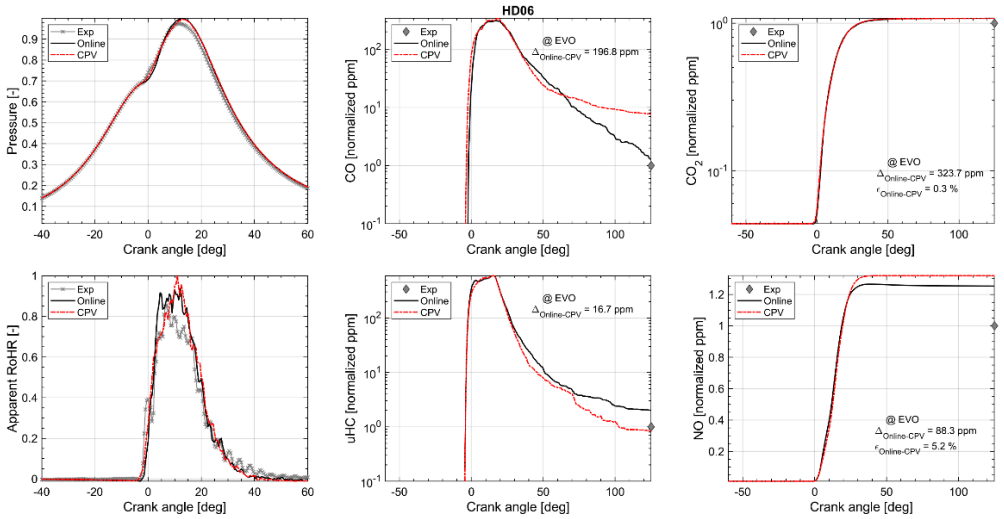

Figure A6. Engine performance and emissions for operating point HD06 (1200 rpm, 14.5 bar IMEP).

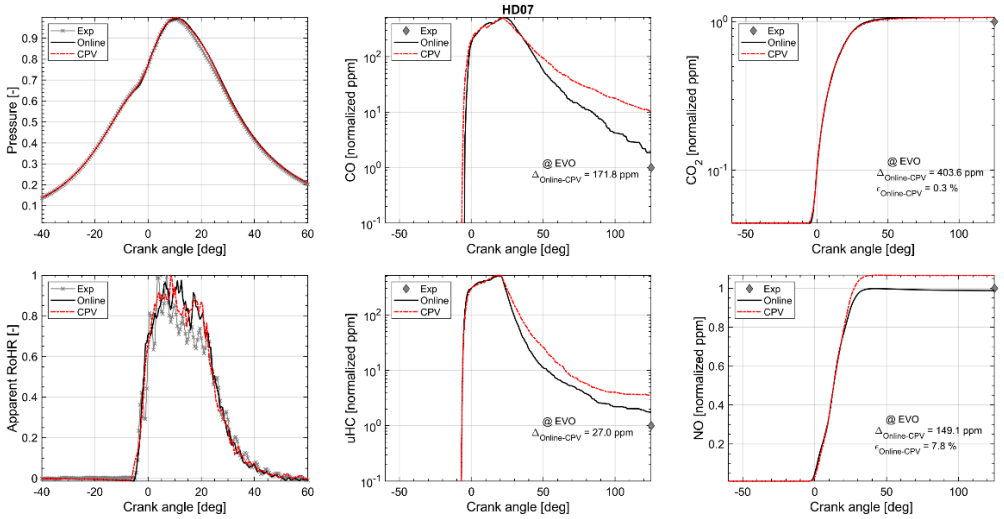

Figure A7. Engine performance and emissions for operating point HD07 (1200 rpm, 22.0 bar IMEP).

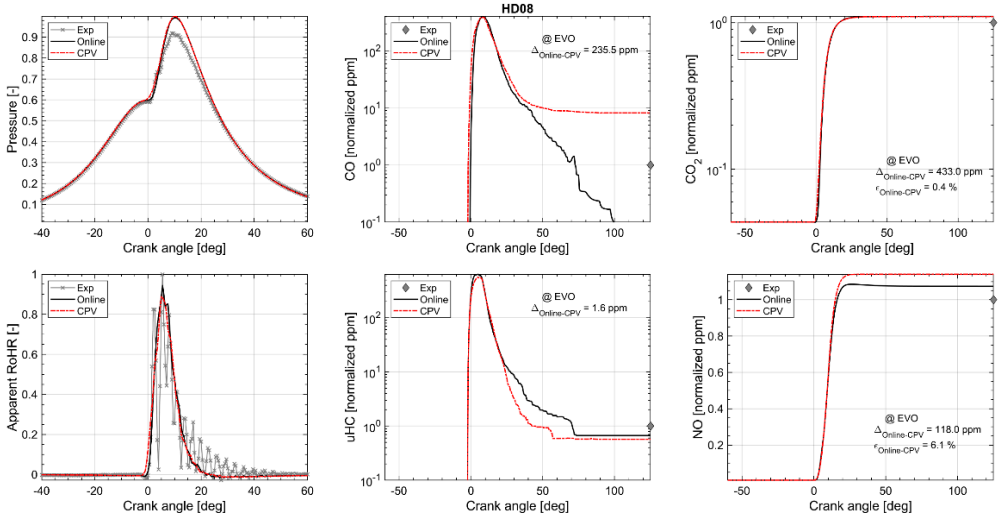

Figure A8. Engine performance and emissions for operating point HD08 (1000 rpm, 6.0 bar IMEP).

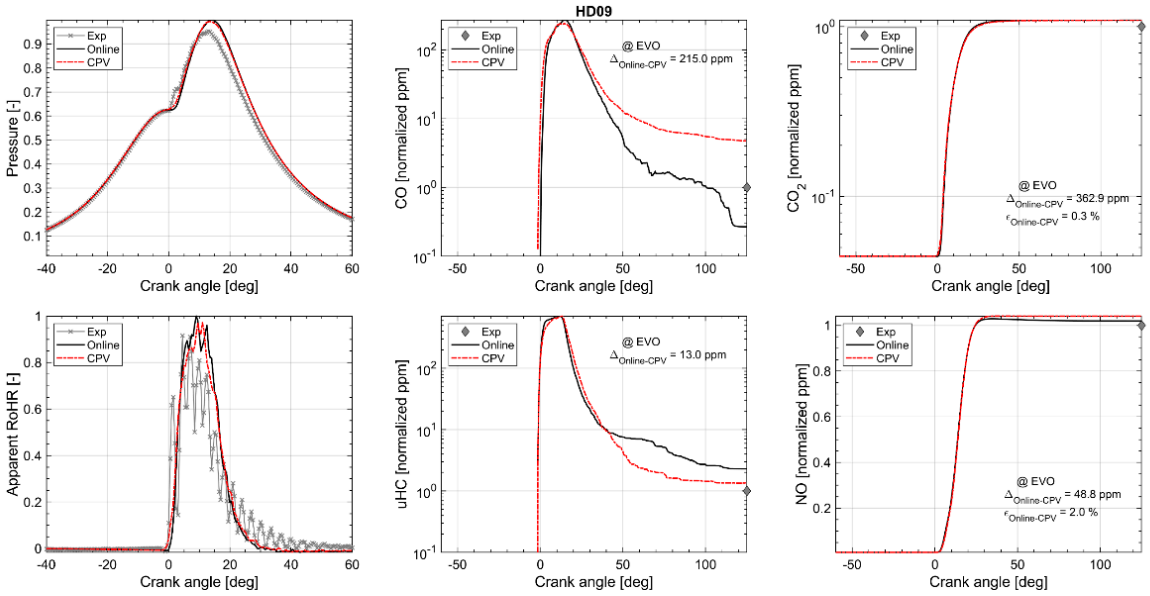

Figure A9. Engine performance and emissions for operating point HD09 (1000 rpm, 11.0 bar IMEP).

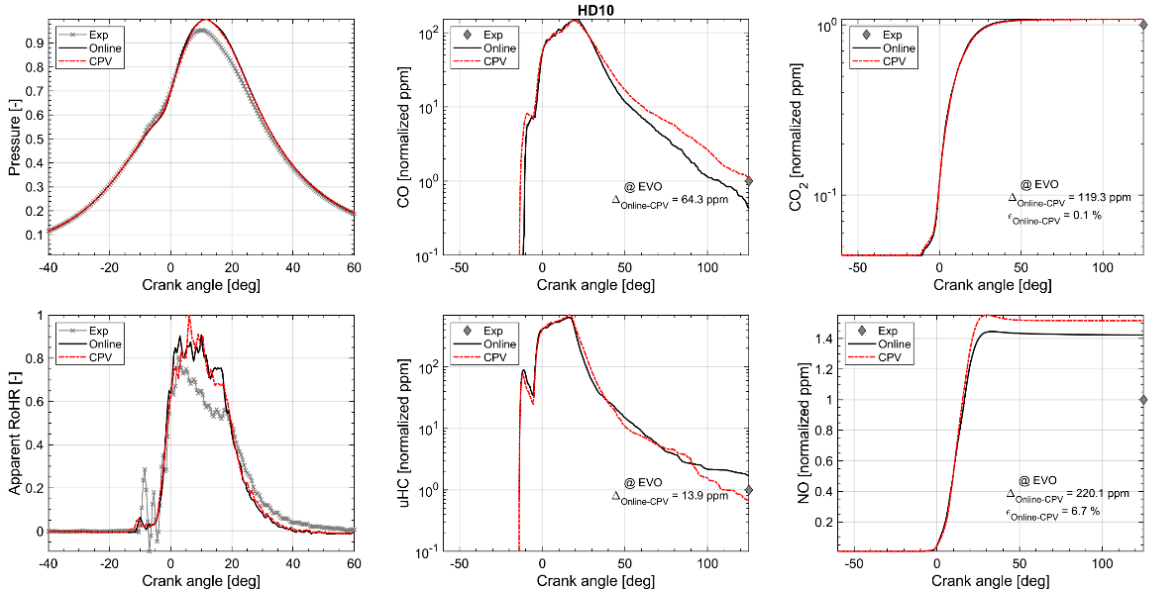

Figure A10. Engine performance and emissions for operating point HD10 (1000 rpm, 22.0 bar IMEP).

Appendix B Spark Ignition Engine Simulation Campaign

In this section, in-cylinder pressure, apparent rate of heat release as well as CO, CO_2 and NO profiles comparisons between experiments and simulations for both solvers are presented for all the spark ignition engine conditions outlined in Error! Reference source not found.

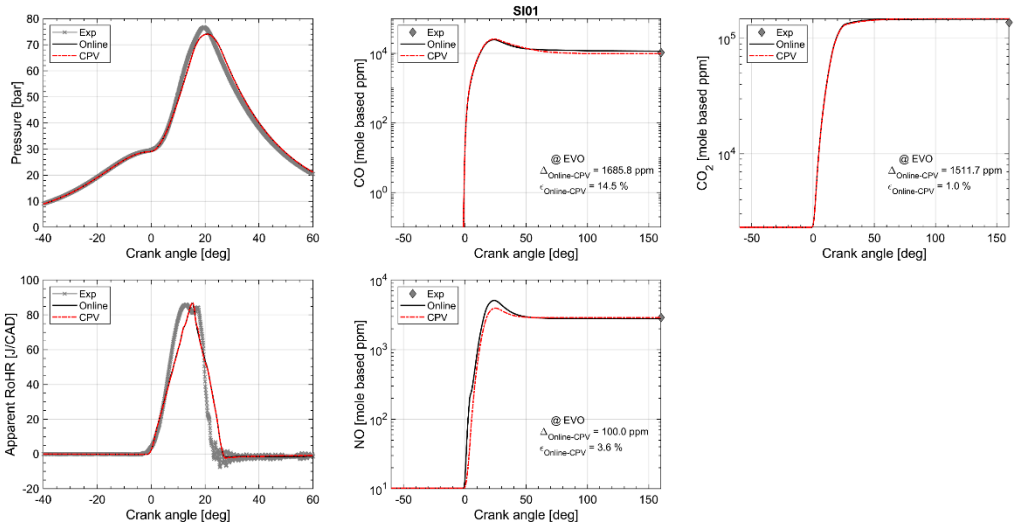

Figure A11. Engine performance and emissions for operating point SI01 (1500 rpm, 15.0 bar IMEP).

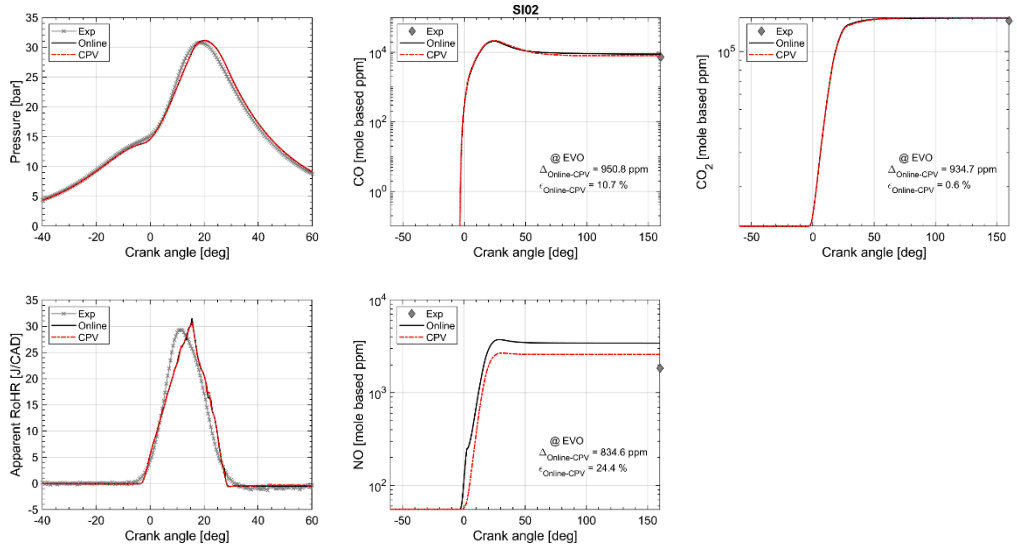

Figure A12. Engine performance and emissions for operating point SI02 (2000 rpm, 5.0 bar IMEP).

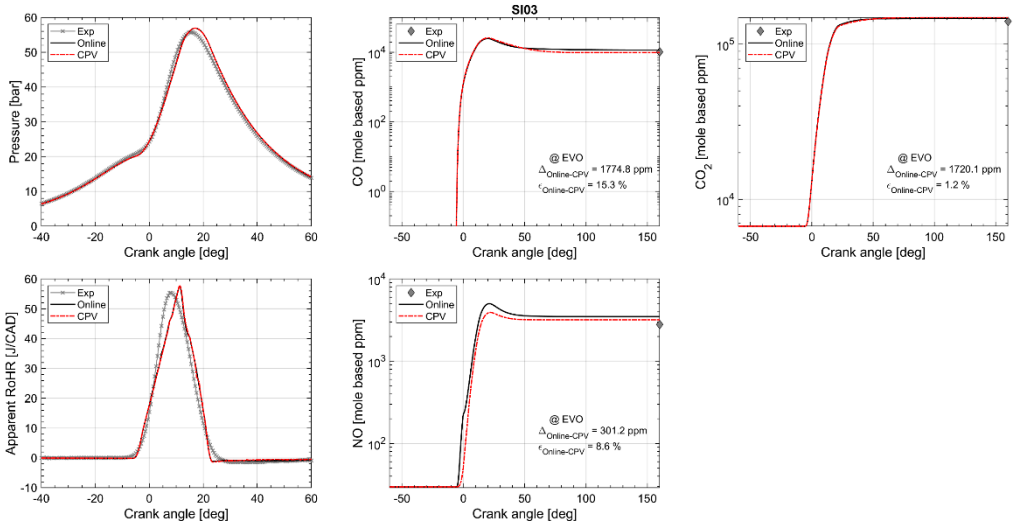

Figure A13. Engine performance and emissions for operating point SI03 (2000 rpm, 10.0 bar IMEP).

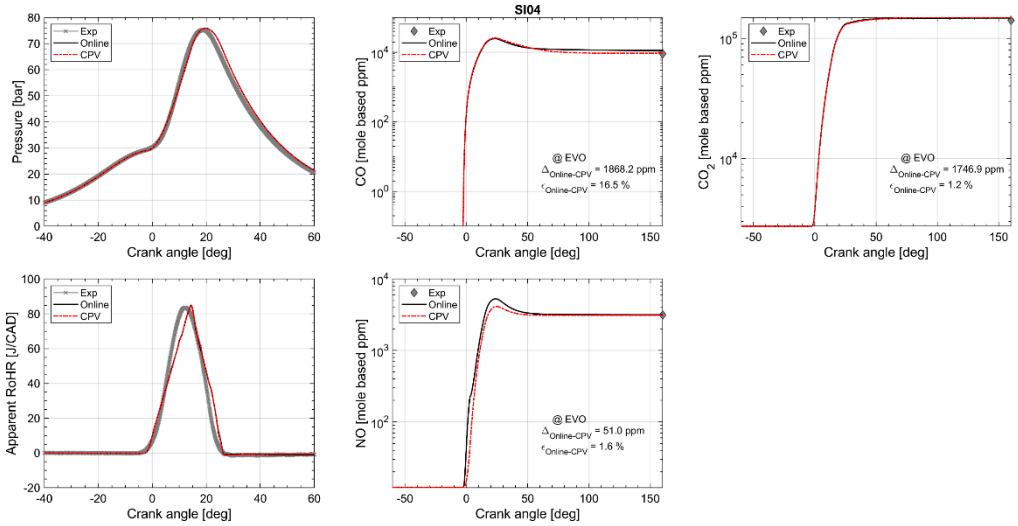

Figure A14. Engine performance and emissions for operating point SI04 (2000 rpm, 15.0 bar IMEP).

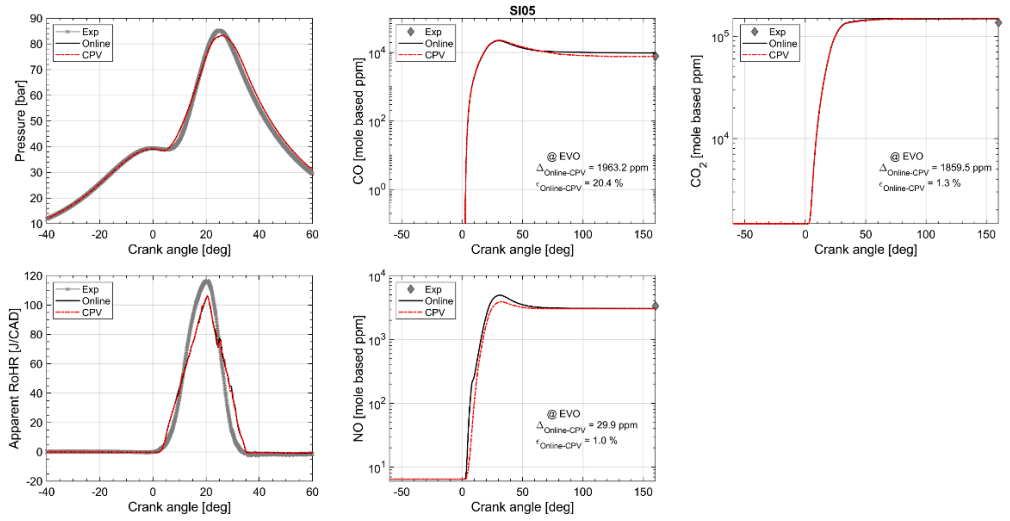

Figure A15. Engine performance and emissions for operating point SI05 (2000 rpm, 20.0 bar IMEP).

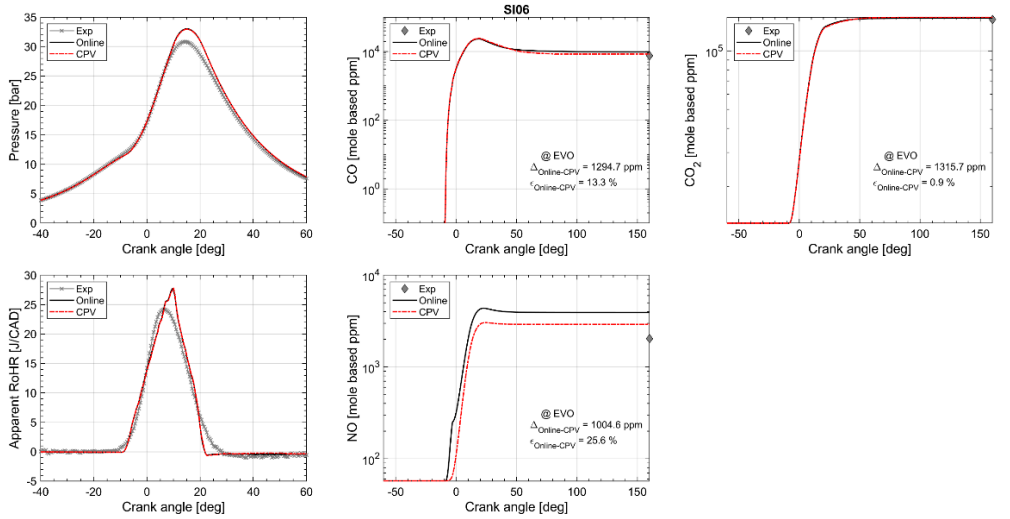

Figure A16. Engine performance and emissions for operating point SI06 (2500 rpm, 5.0 bar IMEP).

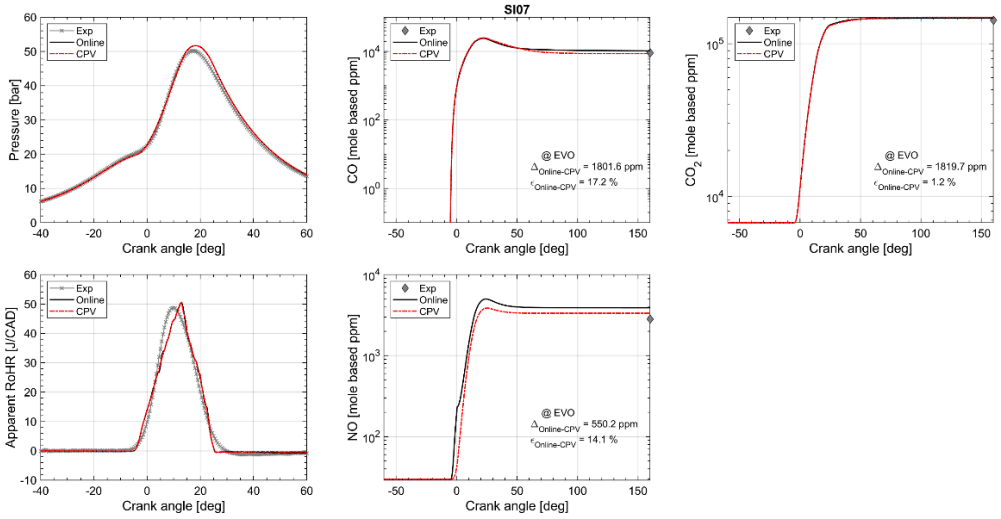

Figure A17. Engine performance and emissions for operating point SI07 (2500 rpm, 10.0 bar IMEP).

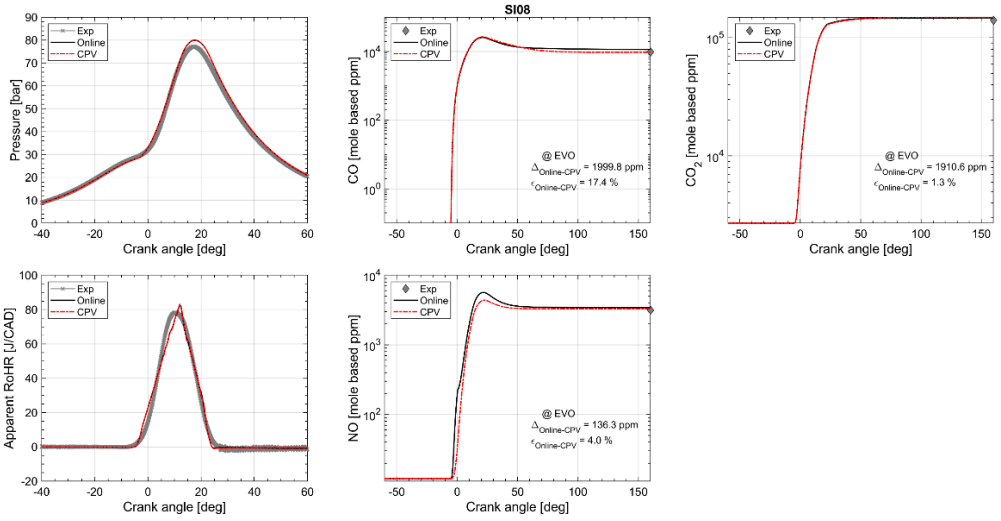

Figure A18. Engine performance and emissions for operating point SI08 (2500 rpm, 15.0 bar IMEP).

References

1. Poulos, S.G.; Heywood, J. The Effect of Chamber Geometry on Spark-Ignition Engine Combustion. In *SAE Technical Paper 830334*; SAE International: Detroit, MI, USA, 1983.
2. Vibe, I. *Halbempirische Formel fur die Verbrennungs-Geschwindigkeit*; Verl. Akad. Wiss. Vd SSR: Moscow, Russia, 1956.
3. Hiroyasu, H.; Kadota, T.; Arai, M. Development and Use of a Spray Combustion Modeling to Predict Diesel Engine Efficiency and Pollutant Emissions: Part 1 Combustion Modeling. *Bull. JSME* **1983**, *26*, 569–575. [CrossRef]
4. Chmela, F.G.; Orthaber, G.C. Rate of Heat Release Prediction for Direct Injection Diesel Engines Based on Purely Mixing Controlled Combustion. In *SAE Technical Paper 1999-01-0186*; SAE International: Detroit, MI, USA, 1999.
5. Nishiwaki, K. A hybrid fractal flame model for si engine combustion comprising turbulent dissipation and laminar flamelets. *COMODIA JSME* **2008**, *8*, 202.
6. Bozza, F.; Gimelli, A.; Merola, S.; Vaglieco, B. Validation of a Fractal Combustion Model through Flame Imaging. In *SAE Technical Paper 2005-01-1120*; SAE International: Detroit, MI, USA, 2005.
7. Jia, M.; Xie, M.; Peng, Z. A Comparative Study of Multi-zone Combustion Models for HCCI Engines. In *SAE Technical Paper 2008-01-0064*; SAE International: Detroit, MI, USA, 2008.

8. Ogink, R.; Golovitchev, V. Gasoline HCCI Modeling: An Engine Cycle Simulation Code with a Multi-Zone Combustion Model. In *SAE Technical Paper 2002-01-1745*; SAE International: Detroit, MI, USA, 2002.
9. Ofner, H.; Schutting, E. Select Assessment of a Multi Zone Combustion Model for Analysis and Prediction of CI Engine Combustion and Emissions. In *SAE Technical Paper 2011-01-1439*; SAE International: Detroit, MI, USA, 2011.
10. Demoulin, F.-X.; Bernard, B.; Lebas, R. A 0D Phenomenological Model Using Detailed Tabulated Chemistry Methods to Predict Diesel Combustion Heat Release and Pollutant Emissions. In *SAE Technical Paper 2011-01-0847*; SAE International: Detroit, MI, USA, 2011.
11. Aceves, S.M.; Flowers, D.L.; Espinosa-Loza, F.; Babajimopoulos, A.; Assanis, D.N. Analysis of Premixed Charge Compression Ignition Combustion with a Sequential Fluid Mechanics-Multizone Chemical Kinetics Model. In *SAE Technical Paper 2005-01-0115*; SAE International: Detroit, MI, USA, 2004.
12. Seidel, L.; Netzer, C.; Hilbig, M.; Mauss, F.; Klauer, C.; Pasternak, M.; Matrisciano, A. Systematic Reduction of Detailed Chemical Reaction Mechanisms for Engine Applications. *J. Eng. Gas Turbines Power* **2017**, *139*, 091701. [CrossRef]
13. Bekdemir, C.C.; Somers, L.B.; De Goey, L.P.; Tillou, J.; Angelberger, C. Predicting diesel combustion characteristics with Large-Eddy Simulations including tabulated chemical kinetics. *Proc. Combust. Inst.* **2013**, *34*, 3067–3074. [CrossRef]
14. Lehtiniemi, H.; Zhang, Y.; Rawat, R.; Mauss, F. Efficient 3-D CFD Combustion Modeling with Transient Flamelet Models. In *SAE Technical Paper 2008-01-0957*; SAE International: Detroit, MI, USA, 2008.
15. Lehtiniemi, H.; Mauss, F.; Balthasar, M.; Magnusson, I. Modeling diesel spray ignition using detailed chemistry with a progress variable approach. *Combust. Sci. Technol.* **2006**, *178*, 1977–1997. [CrossRef]
16. Bo, T.; Mauss, F.; Beck, L.M. Detailed Chemistry CFD Engine Combustion Solution with Ignition Progress Variable Library Approach. In *SAE Technical Paper 2009-01-1898*; SAE International: Detroit, MI, USA, 2009.
17. Fiorina, B.; Gicquel, O.; Vervisch, L.; Carpentier, S.; Darabiha, N. Premixed turbulent combustion modeling using tabulated detailed chemistry and PDF. *Proc. Combust. Inst.* **2005**, *30*, 867–874. [CrossRef]
18. Nakov, G.; Mauss, F.; Wenzel, P.; Steiner, R.; Krüger, C.; Zhang, Y.; Rawat, R.; Borg, A.; Perlman, C.; Fröjd, K.; et al. Soot Simulation under Diesel Engine Conditions Using a Flamelet Approach. *SAE Int. J. Engines* **2009**, *2*, 89–104. [CrossRef]
19. Nakov, G.; Mauss, F.; Wenzel, P.; Krüger, C. Application of a stationary flamelet library based CFD soot model for low-NOx diesel combustion. In Proceedings of the THIESEL Conference on Thermo- and Fluid Dynamic Processes in Diesel Engines, Valencia, Spain, 14–17 September 2010.
20. Karlsson, A.; Magnusson, I.; Balthasar, M.; Mauss, F. Simulation of Soot Formation Under Diesel Engine Conditions Using a Detailed Kinetic Soot Model. In *SAE Technical Paper 981022*; SAE International: Detroit, MI, USA, 1998.
21. Wenzel, P.; Steiner, R.; Krüger, C.; Schießl, R.; Hofrath, C.; Maas, U. 3D-CFD Simulation of DI-Diesel Combustion Applying a Progress Variable Approach Accounting for Detailed Chemistry. In *SAE Technical Paper 2007-01-4137*; SAE International: Detroit, MI, USA, 2007.
22. Da Cruz, A.P. Three-dimensional modeling of self-ignition in hcci and conventional diesel engines. *Combust. Sci. Technol.* **2004**, *176*, 867–887. [CrossRef]
23. Colin, O.; Da Cruz, A.P.; Jay, S. Detailed chemistry-based auto-ignition model including low temperature phenomena applied to 3-D engine calculations. *Proc. Combust. Inst.* **2005**, *30*, 2649–2656. [CrossRef]
24. Knop, V.; Michel, J.-B.; Colin, O. On the use of a tabulation approach to model auto-ignition during flame propagation in SI engines. *Appl. Energy* **2011**, *88*, 4968–4979. [CrossRef]
25. Kosters, A.; Golovitchev, V.; Karlsson, A. A Numerical Study of the Effect of EGR on Flame Lift-off in n-Heptane Sprays Using a Novel PaSR Model Implemented in OpenFOAM. *SAE Int. J. Fuels Lubr.* **2012**, *5*, 604–610. [CrossRef]
26. Lucchini, T.; Della Torre, A.; D'Errico, G.; Onorati, A. Modeling advanced combustion modes in compression ignition engines with tabulated kinetics. *Appl. Energy* **2019**, *247*, 537–548. [CrossRef]
27. Zhou, Q.; Lucchini, T.; D'Errico, G.; Hardy, G.; Lu, X. Modeling heavy-duty diesel engines using tabulated kinetics in a wide range of operating conditions. *Int. J. Engine Res.* **2020**. [CrossRef]
28. Leicher, J.; Wirtz, S.; Scherer, V. Evaluation of an Entropy-Based Combustion Model using Stochastic Reactors. *Chem. Eng. Technol.* **2008**, *31*, 964–970. [CrossRef]

29. Gicquel, O.; Darabiha, N.; Thévenin, D. Laminar premixed hydrogen/air counterflow flame simulations using flame prolongation of ILDM with differential diffusion. *Proc. Combust. Inst.* **2000**, *28*, 1901–1908. [CrossRef]
30. Bougrine, S.; Richard, S.; Michel, J.-B.; Veynante, D. Simulation of CO and NO emissions in a SI engine using a 0D coherentflame model coupled with a tabulated chemistry approach. *Appl. Energy* **2014**, *113*, 1199–1215. [CrossRef]
31. Bozza, F.; De Bellis, V.; Teodosio, L. A Tabulated-Chemistry Approach Applied to a Quasi-Dimensional Combustion Model for a Fast and Accurate Knock Prediction in Spark-Ignition Engines. In *SAE Technical Paper 2019-01-0471*; SAE International: Detroit, MI, USA, 2019.
32. Livengood, J.C.; Wu, P.C. Correlation of Autoignition Phenomena in Internal Comustion Engines and Rapid Compression Machines. *Symp. (Int.) Combust.* **1955**, *5*, 347–356. [CrossRef]
33. Matrisciano, A.; Franken, T.; Perlman, C.; Borg, A.; Lehtiniemi, H.; Mauss, F. Development of a Computationally Efficient Progress Variable Approach for a Direct Injection Stochastic Reactor Model. In *SAE Technical Paper 2017-01-0512*; SAE International: Detroit, MI, USA, 2017.
34. Pope, S. PDF methods for turbulent reactive flows. *Prog. Energy Combust. Sci.* **1985**, *11*, 119–192. [CrossRef]
35. Maigaard, P.; Mauss, F.; Kraft, M. Homogenous charge compression ignition engine: A simulation study on the effect of in-homogeneities. *ASME J. Eng. Gas Turb. Power* **2003**, *125*, 466–471. [CrossRef]
36. Tuner, M. *Stochastic Reactor Models for Engine Simulations*; Lund University: Lund, Sweden, 2008.
37. Bjerkborn, S.; Fröjd, K.; Perlman, C.; Mauss, F. A Monte Carlo Based Turbulent Flame Propagation Model for Predictive SI In-Cylinder Engine Simulations Employing Detailed Chemistry for Accurate Knock Prediction. *SAE Int. J. Engines* **2012**, *5*, 1637–1647. [CrossRef]
38. Pasternak, M.; Mauss, F.; Sens, M.; Riess, M.; Benz, A.; Stapf, K.G. Gasoline engine simulations using zero-dimensional spark ignition stochastic reactor model and three-dimensional computational fluid dynamics engine model. *Int. J. Engine Res.* **2015**, *17*, 76–85. [CrossRef]
39. Netzer, C.; Franken, T.; Seidel, L.; Lehtiniemi, H.; Mauss, F. Numerical Analysis of the Impact of Water Injection on Combustion and Thermodynamics in a Gasoline Engine Using Detailed Chemistry. *SAE Int. J. Engines* **2018**, *11*, 1151–1166. [CrossRef]
40. Heywood, J. *Internal Combustion Engine Fundamentals*; McGraw-Hill: New York, NY, USA, 1988.
41. Franken, T.; Klauer, C.; Kienberg, M.; Matrisciano, A.; Mauss, F. Prediction of thermal stratification in an engine-like geometry using a zero-dimensional stochastic reactor model. *Int. J. Engine Res.* **2019**, *21*, 1750–1763. [CrossRef]
42. Schmitt, M.; Frouzakis, C.E.; Wright, Y.M.; Tomboulides, A.G.; Boulouchos, K. Investigation of wall heat transfer and thermal stratification under engine-relevant conditions using DNS. *Int. J. Engine Res.* **2015**, *17*, 63–75. [CrossRef]
43. Pasternak, M. Simulation of the Diesel Engine Combustion Process Using the Stochastic Reactor Model. Ph.D. Thesis, Brandenburg University of Technology, Cottbus, Germany, 2015.
44. Pasternak, M.; Mauss, F.; Klauer, C.; Matrisciano, A. Diesel engine performance mapping using a parametrized mixing time model. *Int. J. Engine Res.* **2017**, *19*, 202–213. [CrossRef]
45. Kožuch, P. Phenomenological Model for a Combined Nitric Oxide and Soot Emission Calculation in di Diesel Engines. Ph.D. Thesis, University of Stuttgart, Stuttgart, Germany, 2004.
46. Franken, T.; Sommerhoff, A.; Willems, W.; Matrisciano, A.; Lehtiniemi, H.; Borg, A.; Netzer, C.; Mauss, F. Advanced Predictive Diesel Combustion Simulation Using Turbulence Model and Stochastic Reactor Model. In *SAE Technical Paper*; SAE International: Detroit, MI, USA, 2017.
47. Dulbecco, A.; Richard, S.; Laget, O.; Aubret, P. Development of a Quasi-Dimensional K-k Turbulence Model for Direct Injection Spark Ignition (DISI) Engines Based on the Formal Reduction of a 3D CFD Approach. In *SAE Technical Paper 2016-01-2229*; SAE International: Detroit, MI, USA, 2016.
48. Franken, T.; Mauss, F.; Seidel, L.; Gern, M.S.; Kauf, M.; Matrisciano, A.; Kulzer, A.C. Gasoline engine performance simulation of water injection and low-pressure exhaust gas recirculation using tabulated chemistry. *Int. J. Engine Res.* **2020**, *21*, 1857–1877. [CrossRef]
49. Franken, T.; Seidel, L.; Matrisciano, A.; Mauss, F.; Kulzer, A.C.; Schuerg, F. Analysis of the Water Addition Efficiency on Knock Suppression for Different Octane Ratings. In *SAE Technical Paper 2020-01-0551*; SAE International: Detroit, MI, USA, 2020.

50. Breda, S.; D'Adamo, A.; Fontanesi, S.; Giovannoni, N.; Testa, F.; Irimescu, A.; Merola, S.; Tornatore, C.; Valentino, G. CFD Analysis of Combustion and Knock in an Optically Accessible GDI Engine. *SAE Int. J. Engines* **2016**, *9*, 641–656. [CrossRef]
51. Lafossas, F.-A.; Castagne, M.; Dumas, J.P.; Henriot, S. Development and Validation of a Knock Model in Spark Ignition Engines Using a CFD code. In *SAE Technical Paper 2002-01-2701*; SAE International: Detroit, MI, USA, 2002.
52. Ihme, M.; Shunn, L.; Zhang, J. Regularization of reaction progress variable for application. *J. Comput. Phys.* **2012**, *231*, 7715–7721. [CrossRef]
53. Lund Combustion Engineering—LOGE AB. LOGEsoft Products. 2020. Available online: www.logesoft.com (accessed on 14 December 2020).
54. Zeuch, T.; Moréac, G.; Ahmed, S.S.; Mauss, F. A comprehensive skeletal mechanism for the oxidation of n-heptane generated by chemistry-guided reduction. *Combust. Flame* **2008**, *155*, 651–674. [CrossRef]
55. Bekdemir, C.C.; Somers, L.B.; De Goey, L.P. Modeling diesel engine combustion using pressure dependent Flamelet Generated Manifolds. *Proc. Combust. Inst.* **2011**, *33*, 2887–2894. [CrossRef]
56. Wang, X. *Kinetic Mechanism of Surrogates for Biodiesel*; BTU Cottbus-Senftenberg: Cottbus, Germany, 2017.
57. Mauss, F. Entwicklung Eines Kinetischen Modells der Russbildung mit Schneller Polymerisation. Ph.D. Thesis, Rheinisch-Westfälische Technische Hochschule Aachen, Aachen, Germany, 1997.
58. Franken, T.; Duggan, A.; Matrisciano, A.; Lehtiniemi, H.; Borg, A.; Mauss, F. Multi-Objective Optimization of Fuel Consumption and NOx Emissions with Reliability Analysis Using a Stochastic Reactor Model. In *SAE Technical Paper 2019-01-1173*; SAE International: Detroit, MI, USA, 2019.
59. Kauf, M.; Gern, M.; Seefeldt, S. Evaluation of Water Injection Strategies for NOx Reduction and Charge Cooling in SI Engines. In *SAE Technical Paper 2019-01-2164*; SAE International: Detroit, MI, USA, 2019.
60. Netzer, C.; Seidel, L.; Ravet, F.; Mauss, F. Impact of the Surrogate Fromulation on 3D CFD Egnien Knock Prediction Using Detailed Chemistry. *Fuel* **2019**, *254*, 115678. [CrossRef]
61. Franken, T.; Netzer, C.; Mauss, F.; Pasternak, M.; Seidel, L.; Borg, A.; Lehtiniemi, H.; Matrisciano, A.; Kulzer, A.C. Multi-objective optimization of water injection in spark-ignition engines using the stochastic reactor model with tabulated chemistry. *Int. J. Engine Res.* **2019**, *20*, 1089–1100. [CrossRef]

Publisher's Note: MDPI stays neutral with regard to jurisdictional claims in published maps and institutional affiliations.

© 2020 by the authors. Licensee MDPI, Basel, Switzerland. This article is an open access article distributed under the terms and conditions of the Creative Commons Attribution (CC BY) license (http://creativecommons.org/licenses/by/4.0/).